Received: 13 January 2021 | Revised: 22 June 2020 | Accepted: 7 April 2021

DOI: 10.1002/gea.21868

RESEARCH ARTICLE

Geoarchaeology An International Journal WILEY

Mercury enrichment in anthrosols and adjacent coastal sediments at a Classic Maya site, Marco Gonzalez, Belize

Simon Turner[1] | Elizabeth Graham[2] | Richard Macphail[2] | Lindsay Duncan[2] | Neil L. Rose[1] | Handong Yang[1] | Richard Whittet[3] | Cristina Rosique-Esplugas[3]

[1]UCL Geography, London, UK

[2]Institute of Archaeology, UCL, London, UK

[3]Royal Botanic Garden Edinburgh, Edinburgh, UK

Correspondence
Simon Turner, UCL Geography, Pearson Bldg, Gower St, London WC1E 6BT, UK.
Email: simon.turner@ucl.ac.uk

Present address
Richard Whittet, Northern Research Station, Forest Research, Midlothian, UK

Cristina Rosique-Esplugas, UK Centre for Ecology and Hydrology, Midlothian, UK.

Scientific editing by Alyson Thibodeau.

Funding information
Leverhulme Trust

Abstract

Elevated concentrations of total mercury (THg) are found in the surface soils and flanking wetland sediments at the Classic Maya coastal site of Marco Gonzalez, Belize. Significant concentrations (up to 1.3 $\mu g \cdot g^{-1}$ dry mass) of THg occur in leaf litter-rich soils, as well as in the artefact-rich anthrosol spread over the vegetated mound site of structures and occupation debris. The abundance and spatial pattern of major and trace elements measured in the surface soils indicate both site-scale controlling factors of topography, structures and vegetation on soil geochemistry as well as local highs in concentration compared with background, due to human activity. Geochemical stratigraphy of wetland sediment cores shows that a shift from carbonate-reef sediments to mangrove peat in the 13th century AD was attended by an input of allogenic (mineral) elements, including mercury. A THg concentration peak (0.8 $\mu g \cdot g^{-1}$) in brackish pool sediment is ^{210}Pb-dated to 1960–1970 AD, but the incorporation of mercury in multiple cores adjacent to the site shows increasing mercury inputs to have occurred before, during Classic-period Maya occupation and following the sites abandonment. Analysis of element values from site-scale soil sampling, combined with results from off-site cores, provides a numerical framework upon which outlier values of THg and other element spatial patterns can be assessed, especially the spatial co-association of elements related to differences in soil–sediment matrices. Geochemical results from active soils developing from occupation deposits (anthrosols) and sediment cores open up questions concerning contemporary and past mercury accumulation at coastal Mayan sites, and the wider interaction of human and natural biogeochemical processes that occur in human-modified soils and coastal wetland sediments.

KEYWORDS

anthrosols, Belize, mangrove, Maya, mercury

1 | INTRODUCTION

Mercury (Hg) is of particular interest in Maya archaeology due to its use in high-status funerary and cultural practices (Ávila et al., 2014; Batta et al., 2013; Bell, 2007) and what its occurrence in archaeological contexts (floors, middens, ceramic pigments, casques) tells us about artisan industry, commerce and trade in the Mayan world. Multi-element (including mercury) geochemical surveys of Maya archaeological sites have identified significant changes to soil characteristics associated with occupation and industrial activities (Cook et al., 2006; Eberl et al., 2012; Fulton et al., 2017; Lamoureux-St-Hilaire et al., 2019; LeCount et al., 2016; Luzzadder-Beach et al., 2011; Parnell et al., 2002; Terry et al., 2004; Wells et al., 2000).

Marco Gonzalez (MG) is a Classic Maya occupation site at the southern end of Ambergris Caye, Belize (N17.88164, W88.01452) (Figure 1). Exploration for potentially anomalous values of Hg at the site was inspired by the discovery of elemental Hg in a vessel placed beneath the centre of a late 9th–10th century AD ball court at the inland and material culture-linked site of Lamanai (Pendergast, 1982). Connection with Lamanai as well as evidence of longer distance, circum-peninsular trade (Graham & Pendergast, 1989; Guderjan, 1995; Healy, 1989; Lentz et al., 2016; Simmons & Graham, 2017; Simmons et al., 2018) suggests that mercury may also have been traded, passed through or used by Classic Mayan occupants of coastal MG. Even if elemental Hg was never present at MG, the significant amount of Hg (~86%) in its more likely used/traded sulphide mineral form of cinnabar (HgS) (King, 2002) would still be detectable if now incorporated into the artefact-rich anthrosol at the site.

Stratigraphic transects around MG reveal that occupation debris extends from the elevated mound of structures and occupation deposits and is interlayered with a transgressive suite of coastal to wetland sediments, reflecting the sites evolution from more open-marine-influenced to mangrove wetland (Dunn & Mazzullo, 1993).

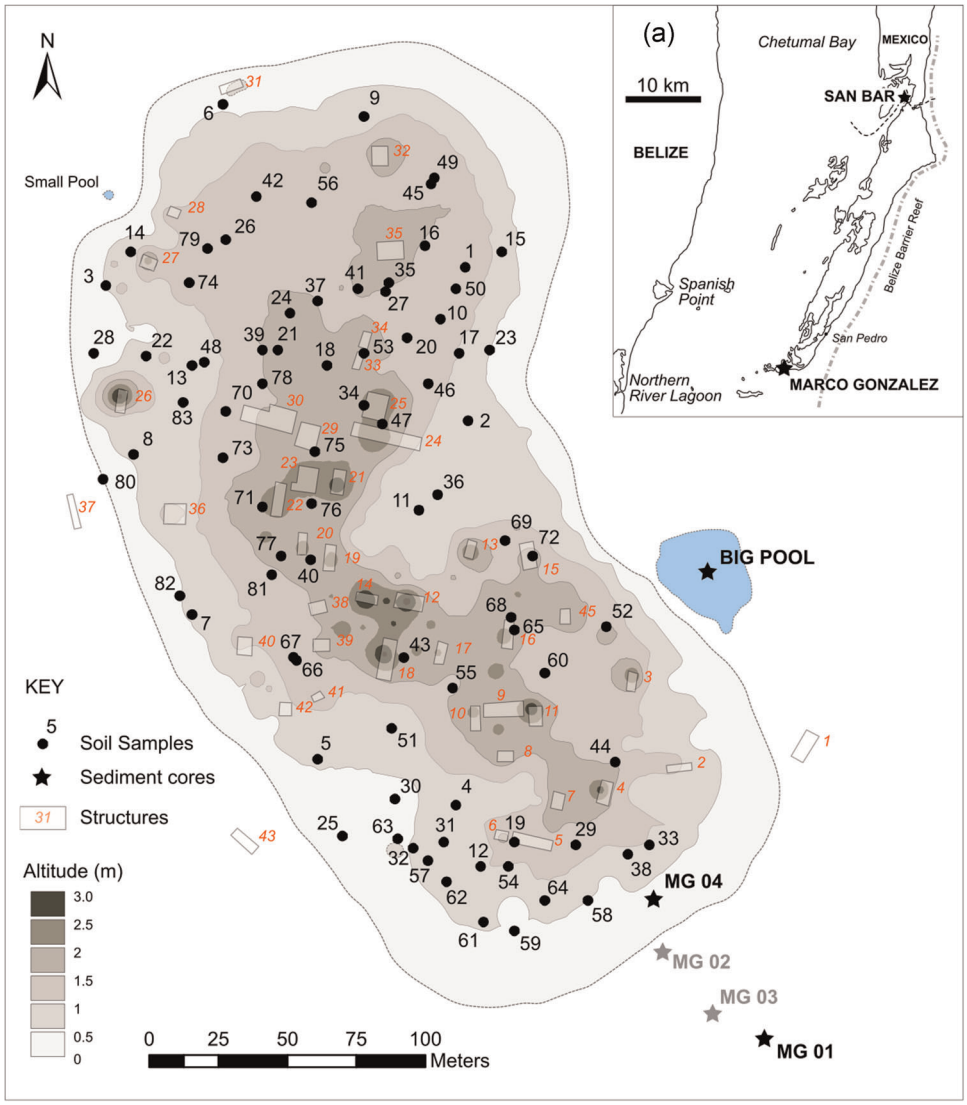

FIGURE 1 Location map of Marco Gonzalez (MG) showing soil sample locations, structures, core sites and ground surface altitude; (a) inset map of MG and San Bar location in relation to Belize [Color figure can be viewed at wileyonlinelibrary.com]

The occupation debris contains materials from the site and the by-products of coastal resource use, indicated by shell and bone remains of fish–shellfish processing and great amounts of ceramic briquetage from intensive salt making (Graham et al., 2017).

Coastal wetland sediment sequences have been used extensively to investigate historical human activity, using mercury and trace metal sediment records, at both global and local scales (Conrad & Sanders, 2017; Gan et al., 2013; O'Shea et al., 2018; Rosales-Hoz et al., 2003; Silva et al., 2003; Wang et al., 2018). Mercury in coastal wetland and estuarine sediments is of significant interest due to its presence from often unambiguous historical industrial sources and its pervasive accumulation through food webs (Cotin et al., 2011; Elbaz-Poulichet et al., 2011; Kongchum et al., 2006; Mitchell & Gilmour, 2008; O'Driscoll et al., 2011). Mercury is of particular biogeochemical and toxicological interest in mangrove–coral and human ecosystems due to distinct food-web interactions (high biomagnification) and chronic health risks associated with the consumption of reef fish (M. F. M. Costa et al., 2012; Guzmán & García, 2002) and mangrove areas converted to aquaculture (B. Costa et al., 2013; Lacerda et al., 2011). Understanding long-term anthropogenic and natural Hg cycling with contemporary sediment accumulation dynamics is also important, especially in relation to future remobilisation of colonial and legacy industrial Hg inputs to coastal zones (Fitzgerald et al., 2018; O'Shea et al., 2018; Rúa et al., 2014).

The closest comparable study to this paper is archaeological and geochemical survey work conducted at the Chan b'i Salt Works in southern Belize (McKillop, 2005; Sills & McKillop, 2018; Sills et al., 2016). At the now submerged Mayan site, evidence of salt production exists in the form of preserved wooden structures and abundance of remains (briquetage) from intensive salt making by heating brines in ceramic vessels from the Classic Maya period (300–900 CE). Surface samples of seafloor mangrove peat sediment reveal variations of major elements in relation to inferred structures and working activities. Variations in phosphorus, magnesium and potassium occur near structures where salt was evaporated, and common minerogenic elements are enhanced from the dumping of briquetage. Trace elements in the sediments show little variation and are low in concentration (compared with mean crustal values), due to the mangrove peat origin of the sediment and apparent only industrial occupation of the site, for example, no use of metal-containing pigments in wall plasters or ceramic pigments. A direct comparison of mercury concentrations found (maximum 0.001 $\mu g \cdot g^{-1}$; E. Sills [personal communication, 2020]) is not possible with this study, due to the partial digestion extraction technique chosen to investigate the anthropogenic component of the sediment in Chan b'i. Nonetheless, the very low values of mercury measured at Chan b'i suggest that it was not present at the site during occupation (mirroring the lack of other residential wastes) or enhanced by geological or ecological bioaccumulation processes.

This paper provides a site-scale geochemical assessment of spatial patterns of total mercury (THg) and other elements in anthrosols, with downcore trends in wetland sediments to identify temporal patterns due to human modification during and after occupation at MG. Before more detailed soil analyses occur, work such as this should be considered the first step for geoarchaeological–geochemical survey work to improve on the often tentative or highly ambiguous interpretations of element assemblages to distinct activities (Entwistle et al., 1998). Outside of well-defined archaeological contexts, the identification of Hg and other trace element anomalies due to human activity is complicated because natural geological and biogeochemical sources and depositional and post-depositional processes can result in local spatial and temporal heterogeneity. Uncertainties in the causes of mercury enrichment can be reduced by co-investigation of trace elements such as Cu, Zn, Pb and Ni that have more limited sources and perseverance in archaeological materials (Cook et al., 2006). A contaminant mapping/geochemical prospecting approach using surface soil samples is used here, to provide both potential new sites for further excavation and, perhaps more important, sufficient numerical values with which to appropriately explain element values in and around archaeological contexts and anthrosols as significantly high or low and due to human activities (Oonk et al., 2009; Reimann et al., 2005; Wilson et al., 2008). Measurements of total abundance of mercury and other elements are used in this study, as natural geological sources of elements (including mercury) at the site were considered minimal due to the site's coral-limestone caye location with scarce/absent terrigenous soils (Dunn & Mazzullo, 1993; Ebanks, 1975; Graham & Pendergast, 1989). It is recognised that total element values will be higher in soils where total extraction and total abundances combine both natural and human inputs, compared with studies using partial extraction techniques that have been widely used in Mayan soil/anthrosol studies (Fulton et al., 2017; LeCount et al., 2016; Sills et al., 2016; Terry et al., 2004). Whichever analytical techniques are chosen and whether total or partial abundances of Hg are measured, at the site scale, it is the spatial or temporal (downcore) patterns of trace elements that are important rather than the absolute values for archaeological and paleoenvironmental interpretation (Wells et al., 2000).

1.1 | Site description

MG is in the coral island, back-barrier and lagoon complex of Chetumal Bay and the Belize Barrier Reef. Chetumal Bay is a large, shallow (1098 km^2, max. 3.5 m depth) hyposaline bay with a limestone-dominated catchment draining northern Belize, Guatemala and Mexico. MG is approx. 1 km from the reef edge, in the lee of the prevalent east and south-easterly trade winds. Hurricanes and tropical storms are a regular occurrence along the coast (Denommee et al., 2014; Gischler et al., 2008). Annual rainfall is ~1600 mm with a mean air temperature of 26°C (www.hydromet.gov.bz). Tidal range at Ambergris Caye is <0.5 m. MG forms a distinct topographic high (max. 4 m above sea level) amongst the surrounding *Rhizophora* sp. mangrove. The vegetation community of the raised site (ca. 6.6 ha) contains non-littoral and broadleaf species of a Belize 'Caye Forest' (Murray et al., 1999)

The site contains a preserved record of Mayan coastal occupation from the Pre-classic (ca. 300 BC) to Post-classic period (ca. AD 1500). Activities over time are reflected in the remains of maritime resource exploitation, domestic and larger scale refuse and construction of platforms (using reefstone and sandstone) that supported perishable buildings, preserved floors, inhumations and a locally distinct elevated land surface formed of occupation-generated waste products. Investigation of archaeological sequences, soils and sediments at MG was carried out during 2013–2014 (Graham et al., 2017) after excavations at the site in 1986, 1990 and 2010 (Graham & Pendergast, 1989; Graham & Simmons, 2012). Stratigraphic evidence from the site supported by micromorphological and geochemical analyses (Macphail et al., 2016) has revealed an approximately three-part succession: (i) ash and bone-rich colluvium and lime plaster floors that accumulated (~1 m thick) over a natural elevation of Pleistocene reef limestone in the Terminal Pre-classic to Early Classic periods (AD 1–300); (ii) further ground raising (approx. 1 m) in Late Classic times (ca. AD 550–760) as the result of the accumulation of lime floors, burnt shell and charcoal-rich ash layers related to salt processing along with marine fish and shellfish products; and (iii) accumulation of occupation debris (i.e., conch shells, fish bones, ceramics and inhumation remains) and a biologically worked anthrosol intercalated with Late Classic deposits to form the surface soil present today (Dunn & Mazzullo, 1993; Graham & Pendergast, 1989). Analysis of the surface anthrosols ('dark earths') shows that finely fragmented charcoal contributes to the dark coloration more than the organic carbon content (Macphail et al., 2016). Non-local lithics such as slate, quartzite, pumice and other volcanic and metamorphic stones occur at low frequencies in MG archaeological deposits (Duncan, 2019; Graham & Simmons, 2012). Mercury measurements (THg) from test-pit stratigraphic samples show a clear enhancement in upper (2–3 cm below surface) horizons, whereas concentrations of trace metals often associated with human activity (nickel (Ni), copper (Cu) and zinc (Zn)) in the same horizon are comparable to deeper occupation deposits (Macphail et al., 2016). The upper horizon increase of THg supports the pattern seen in the following surface soil results, but the lack of enrichment measured in deeper layers needs to be considered as having come from only a limited two-dimensional extent of archaeological contexts, compared with previous work on excavated surfaces and floors that show significant spatial heterogeneity of trace elements.

2 | METHODS

2.1 | Field surveying and sampling

The term 'soil' is used to define samples collected higher than the local vertical elevation of coastal mangrove, and 'sediment' from or beneath the mangrove surface. Soil samples were collected over a 4-day period in August 2013. Randomly generated coordinates were entered into a GPS unit to avoid bias between observed soil composition, proximity to structures and vegetation types. Soil sample locations in the mangrove were not collected to restrict collection to potential anthrosol material rather than modern surface peat. Sample location recording was occasionally compromised under dense foliage using a handheld GPS unit (Garmin e30). Locations affected by loss-of-satellite reception were recorded as last known position showing an error of 3 m. Locations were verified on site with reference to the archaeological survey (Graham & Pendergast, 1989) and desk-based confirmation with GPS measurements of ground features visible in Google Earth.

At each surface soil location, a small hole was dug with a stainless-steel knife and an ~10-g soil sample was removed from the side wall at 5–10 cm below ground surface. This interval was recognised during sampling as a compromise between collecting many samples in a short space of time, from a land surface with evidence of vertical mixing (crab burrows, tree throw and looters pit spoil) against measuring multiple depths in heterogenous soils to fully establish parent material inputs (Ander et al., 2013; Fordyce et al., 2005). Avoiding the very surface 5 cm was also considered to limit the effect of recent deposition of trace metals from atmospheric deposition and burning of waste. Bonfires to burn waste, machete sharpening and disposal of batteries (Golden et al., 2015; Terry et al., 2004) are capable of creating lasting geochemical signatures in soils. Corroded batteries or other burnt waste was not noted during the survey.

Mangrove and coastal sediments were sampled using a hand-operated steel gouge of 1-m length (60-mm diameter; Van Walt Ltd.). Four cores (MG01–MG04) along an ~100-m NW–SE transect were collected (Figure 1) where interlayered anthrosols, lagoon muds and sands and mangrove peats had been previously mapped (Dunn & Mazzullo, 1993). Cohesive mangrove peat and muds were collected with minimal compaction, but subsurface water-saturated sands were poorly collected below 1-m depth. After core description (Munsell colour, visual grain size/sorting and clast types), consecutive 1-cm downcore intervals were sampled from both MG01 and MG04 using a stainless-steel spatula on the core interior, following removal of mud smeared on the exterior during core extraction. A short (0.63 m) core was extracted from the centre of the pond (MG Big Pool, BP) (Figure 1) to the east of the site using a raft and Livingstone piston corer in 0.48-m water depth. The decision to analyse a lentic core from 'Big Pool' was based on determining its waterbody origin and its potential to contain a complementary aquatic sediment record to compare with mangrove deposits. The core was sliced using a stainless-steel blade at 1-cm intervals. A surface sample (0–2 cm) was also collected by a Livingstone core tube from a small mangrove pool ('Small Pool') to the NW (Figure 1). A short soil core (21-cm depth) was collected from a recently formed caye 'San Bar (SB)' (N18.187187, E87.869324, see Figure 1a) to provide regional element values unaltered by human occupation (Figure S1). Recently fallen leaves and bulk leaf litter samples were also collected in August 2013. These were collected around MG from beneath a selection of tree and shrub species for preliminary data on

leaf litter inputs of metals to soils. All soil, sediment and vegetation samples were sealed in PVC bags and kept in dark and refrigerated, before shipment (September 2013) to the United Kingdom.

2.2 | Surveying and GIS methods

The theodolite-derived map of structures and elevation spot heights (Graham & Pendergast, 1989) was digitised and georeferenced for GIS using ground control point coordinates measured by GPS during fieldwork and features visible in Google Earth. Inverse distance weighted interpolation of surveyed spot heights generated a raster grid (1-m cells) from which values of metres above sea level (m.a.s.l.) were applied to soil sample locations contained in the cells. A levelling survey conducted on August 8, 2013 from the site datum to the sea confirmed the mangrove surface at or near sea level. Preliminary vegetation mapping of MG took place in August 2014 using multiple 10 × 10 m plots, with species recorded using a DAFOR scale of abundance. The centre point of the quadrat was recorded by hand-held GPS. Distances between structures and soil samples are calculated to the nearest edge of the structure-defining polygon.

2.3 | Laboratory methods

All samples were refrigerated (4°C) and then frozen after initial textural analysis (LOI, below) from September 2013 to January 2014. Freeze-drying occurred during the period October 2013 and March 2014 to minimise Hg loss by microbiological activity and/or drying (Hojdová et al., 2015). After freeze-drying, large fragments of ceramics, wood, pumice and shell were removed from the soil and sediment samples. The <125-μm fraction was retained for analysis by passing the freeze-dried sample through a stainless-steel sieve. Sieves were washed with mild detergent and deionised water and air-dried between samples. The <125-μm fraction was milled with an agate pestle and mortar that was cleaned with deionised water, rinsed with acetone and dried between samples.

The <125-μm fraction of soil and sediments were measured for THg, and 0.2 g of sample (4 d.p.) was digested in concentrated HCl and HNO_3 (molar ratio 3:1; aqua regia) for 2 h at 100°C in overnight acid-leached 50-ml polypropylene tubes. Digested solutions were measured using cold vapour atomic fluorescence spectrometry (CV-AFS), following reduction with $SnCl_2$. Reference sediment samples (IGGEC-GBW07305, certified value 0.10 ± 0.02 $\mu g \cdot g^{-1}$ dry mass) and aqua regia blanks were digested with sample batches. Certified sediment samples measured 0.106 ± 0.004 ($n = 4$), 0.103 ± 0.003 ($n = 4$) and 0.102 ± 0.003 ($n = 4$). Quality control samples using dilutions of certified reference mercury standard (TraceCERT®; Sigma-Aldrich: 1000 ± 4 $ng \cdot L^{-1}$) were measured every five samples to monitor measurement stability during machine running. Digested samples, standards and quality control samples were introduced into the CV-AFS after flushing with matrix-matched aqua regia and deionised water blank. Measurements of THg concentration were continuously monitored to zero before the introduction of next sample, thus preventing carryover of values between measurements.

X-ray fluorescence spectroscopy (XRF) is an expedient, non-destructive method of obtaining multi-element data from bulk soil and sediment samples. Two grams (4 d.p.) of milled sediment was weighed into nylon pots with a Mylar film base and compressed using a nylon die. Reliable elemental values of Mg, Al, Si, P, K, Ca, Ti, V, Cr, Mn, Fe, Ni, Cu, Zn, As, Br, Rb, Sr, Y, Zr, Ba and Pb were obtained with co-measured certified reference sediments (NIST RM 8704 and CANMET LKSD-2). Recovery rates for Ni, Cu, Zn and Pb were 105%–96%, 107%, 102%–104% and 99%–103%, respectively. Soil samples were measured for magnetic susceptibility (χlf) using a Bartington MS2 sensor following XRF analysis.

Bulk organic content for soil and sediment samples was determined gravimetrically by loss on ignition (LOI) (Dean, 1974; Heiri et al., 2001). A 0.5-g subsample was dried at 105°C for 12 h and weighed before being combusted at 550°C (LOI^{550}) for 2 h in a muffle furnace. LOI^{550} may be used as an estimate for total organic carbon (TOC%) by multiplying LOI^{550} by 0.469 (Dean, 1974). An LOI^{550}-based estimate of %TOC is, however, limited with low-organic soils/sediments (<10% LOI^{550}) due to water loss from mineral lattices, so only LOI^{550} values were used in this analysis. An estimate of bulk carbonate (% CO_3) content of the mangrove and pool cores was also assessed following higher temperature (950°C) combustion and weighing (LOI^{950}) (Heiri et al., 2001).

Fresh leaf litter samples were rinsed with deionised water to remove dust before being freeze-dried and homogenised by pestle and mortar. Also, 0.2-g subsamples were digested in aqua regia for THg analysis as described for soils and sediments and in 6 ml concentrated nitric acid (HNO_3) only for ICP-OES analysis for Ni, Cu, Zn and Pb.

To provide more information on changing depositional environments at the margin of MG, Big Pool core samples were selected for diatom analysis. Diatom (Bacillariophyceae) fossil records are used in transitional coastal settings to identify fluctuations between marine, freshwater and terrestrial conditions and impacts of human activity during coastal wetland development (Pande et al., 2015; Parsons et al., 2006; Vos & de Wolf, 1993). Diatoms are used as ecological indicators of significant metal contamination in aquatic environments (Morin et al., 2012) but at low concentrations, co-effects of nutrients, salinity and substrate dominate coastal diatom assemblages (Desianti et al., 2017, 2019; Pande et al., 2015). Sediment samples (0.1-g dry mass) were placed in 20 ml of 30% H_2O_2 and heated in a beaker on a hot plate (90°C, ~2 h) to oxidise organic material. A repeat treatment of H_2O_2 was necessary in samples of 0–20 cm due to abundant organic matter. Cooled samples were treated with dilute HCl (50%) to remove the remaining H_2O_2 and carbonate matter, before being rinsed with distilled water into 10-ml tubes. The samples were centrifuged (1200 rpm) and rinsed (×3) with distilled water. Clay was removed during the last wash by adding weak (1%) ammonia (NH_3) and decanted with the supernatant. Aliquots of each sample (0.5 ml) were pipetted on 19-mm coverslips and allowed to dry at room temperature, before being mounted on slides using

Naphrax (refractive index ~1.7). Diatom identification and ecology followed (Krammer & Lange-Bertalot 1988, 1991; Stidolph et al., 2012).

2.3.1 | Sediment core chronologies

Freeze-dried, milled sediment samples from the MG Big Pool core were analysed for ^{210}Pb, ^{226}Ra, ^{137}Cs and ^{241}Am by direct gamma assay. Sediments were placed in air-tight containers for 3 weeks before counting to allow radioactive equilibration. The isotope ^{210}Pb is measured by its gamma emissions at 46.5 keV, and ^{226}Ra by the 295 and 352 keV gamma rays emitted by its daughter isotope ^{214}Pb. Caesium-137 and ^{241}Am were measured by their emissions at 662 and 59.5 keV, respectively (Appleby et al., 1986). Corrections were made for the effect of self-absorption of low-energy gamma rays within the sample (Appleby et al., 1992). Radionuclide dating of the Big Pool core was complemented by spheroidal carbonaceous particle (SCP) analysis (Rose, 2008; Rose & Juggins, 1994). Two samples were submitted to Queens University, Belfast, for radiocarbon analysis to provide rangefinder dates for the carbonate mud-to-organic (mangrove) peat transition: a charcoal fragment in the Big Pool core at 33–34 cm (UBA-27742) and bulk peat at 62–63 cm in core MG01 (UBA-27743).

3 | RESULTS

3.1 | Surface soil data

Descriptive and robust summary statistics were calculated (mean, H^{15} mean and median absolute deviation [MAD]) (Table 1). Preliminary descriptive statistical tests (one-sample Kolmogorov–Smirnov, Shapiro–Wilk) on the range of element values from the 83 surface soil samples show both normal and nonparametric distributions (Table 1 and Figure S2), emulating the mapped variation of elemental abundances across the site (Figures S3–S7). All element concentrations, unless specified, are expressed as dry mass ($\mu g \cdot g^{-1}$ or %). Spatial maps of the data using bubble maps, where the diameter of the sample spot corresponds to the concentration of an element, were produced using ArcMap 10.3 (Figures S3–S7).

THg concentrations in MG surface soils ($n = 83$) range from 0.05 to 1.33 $\mu g \cdot g^{-1}$ (mean, 0.208; *SD*, 0.178) (Figures 2 and S8). The mean THg of measured MG surface soils is four times higher than mean upper crustal concentrations (MUCC) of 0.05 $\mu g \cdot g^{-1}$ (Rudnick & Gao, 2003). Sample points SF52 and SF76 are noticeable highs (0.78 and 1.33 $\mu g \cdot g^{-1}$, respectively) but occur in different soil matrices and locations. SF52 had an abundance of ceramic sherds, conch shells, obsidian, fish vertebrae and charcoal and low-organic content (LOI^{550}, 17.1%), whereas SF76 near the centre and highest area of the site is a leaf litter-rich forest soil (LOI^{550}, 44%). The next two highest soil THg values (SF67, SF75) also come from contrasting matrices. The lowest THg soil values (<0.1 $\mu g \cdot g^{-1}$) are found fringing the site, upslope of the mangrove margin beneath *Spartina* sp. vegetation (Figure 2). THg values are only positively correlated (Spearman's) with Mn (0.3), χlf (0.17), Cu (0.14) and LOI^{550} (0.16) (Figure S9).

Mean surface soil concentrations of lithogenic, mineral lattice elements (e.g., Si, K, Al, Rb, Fe, Zr and Ba) are lower as compared with MUCC (Table 2). Carbonate-associated (Ca, Sr) and organic/vegetation-associated elements (P, Br) are conversely higher. These concentrations are not unsurprising in soils on a vegetated barrier–caye developed on a Pliocene–Holocene carbonate platform (Adomat & Gischler, 2015; Gischler & Hudson, 2004; Mazzullo, 2006). Mean metal element concentrations also vary, either lower than MUCC (Fe, V, Cr, Ni and Pb) or broadly comparable to MUCC (Cu, Zn and Sn).

Comparison of MG soil element values with soil values from the unoccupied, vegetated caye SB (Table 2) provides a more appropriate measure of how different MG soils are in the Chetumal Bay–Ambergris caye landscape. Mean MG soil values of almost all elements are greater than SB (Table 2). Mean Ca% is lower in MG soils than SB due to the shell-rich matrix of SB. A local enrichment process of mercury in the surface soils of MG is indicated by THg values four times higher than SB soil (mean, 0.04; *SD*, 0.01 $\mu g \cdot g^{-1}$).

Skewed and nonparametric distributions (Table 1) illustrate the spatial variation of elemental abundances measured across MG. A divide occurs between normally distributed lithogenic/biogenic elements and elements with a skewed distribution, including those often associated with anthropogenic enrichment (Hg, Cu, P and Pb). Correlation values (Figure S9) between elements and LOI^{550} suggest that the differences among the surface soils at the site are due to a scale of mixing between organic, lithogenic and Ca/Sr-dominant endmembers. A significant correlation occurs between lithogenic-associated elements (Si, Ti, Fe, Al, Rb and Y), indicating a common source. The negative correlation of Ca and Sr values with lithogenic elements suggests they are associated with biogenic carbonate (shell and reef limestone) materials.

Variations in physical and geochemical sediment properties can be the dominant cause of trace metal variance, especially where the effects of anthropogenic alteration may be subtle. The chemistry and large surface area of fine-grained sediment (clays) and organic matter provide a high sorption capacity for contaminants in aquatic and soil systems. Hg and trace metals tend therefore to be found in finer grained and organic-rich sediments. Associations between trace metals/metalloids and high Al (as proxy for fine-grained mineral sediment) are apparent in a multiple covariate graph (Figure S10), especially for As and Ni. Also evident is the association of Cu and Zn and the identification of metal outliers related to high LOI^{550}, χlf and Al (SF76, SF53 and SF52).

3.1.1 | MG soil element enrichment factors (EFs)

EFs of metals commonly elevated by anthropogenic activity were calculated by comparison to both global crustal background and

TABLE 1 Element concentration values in surface soil samples, Marco Gonzalez

									One-sample KS			SW
		Min.	Max.	Mean	Median	*SD*	H_{15}	MAD	Coeff.	*p*	H_0	H_0
	χlf	0.03	31.8	3.9	1.03	6.5	2.2	0.8	0.27	0.00	No	No
	LOI^{550}	8.3	46.9	18.8	17.9	7.1	18.2	4.9	0.08	0.17		No
%	Mg	1.2	3.69	2.2	2.2	0.6	2.2	0.4	0.05	0.20		
	Al	1.1	4.74	2.9	3.0	0.8	2.9	0.5	0.08	0.20		
	Si	2.5	8.45	5.7	5.9	1.2	5.8	0.6	0.14	0.00	No	No
	P	0.3	2.64	0.7	0.6	0.3	0.6	0.1	0.17	0.00	No	No
	K	0.02	0.47	0.3	0.3	0.1	0.3	0.05	0.04	0.20		
	Ca	10.2	35.15	23.7	24.0	4.6	23.8	3.4	0.04	0.20		
	Ti	0.05	0.23	0.14	0.1	0.03	0.1	0.020	0.07	0.20		
	V	0.00	0.02	0.01	0.01	0.003	0.005	0.002	0.06	0.20		
	Cr	0.00	0.01	0.01	0.01	0.002	0.01	0.002	0.05	0.20		
	Mn	0.00	0.02	0.01	0.01	0.003	0.01	0.002	0.09	0.60		No
	Fe	0.3	1.4	0.94	0.96	0.2	0.94	0.1	0.10	0.18		
$\mu g \cdot g^{-1}$	Ni	1.6	34.6	15.8	16.3	7.7	15.8	5.8	0.08	0.20		
	Cu	8.9	61.3	23.7	23.2	7.0	23.3	3.7	0.11	0.00	No	No
	Zn	20.7	216.2	59.4	52.2	27.2	54.5	6.7	0.23	0.00	No	No
	As	0.6	39.6	17.3	17.9	9.2	17.1	7.6	0.07	0.20		
	Br	127.3	387.0	206.6	202.3	46.7	203.3	28.9	0.07	0.20		No
	Rb	3.4	15.8	10.0	10.0	2.1	10.1	1.3	0.05	0.20		
	Sr	1108	4394	2630	2593	587	2616	346	0.07	0.20		
	Y	2.0	23.7	13.4	13.9	4.7	13.6	3.0	0.09	0.06		
	Zr	21.0	88.1	54.6	54.8	12.4	54.6	7.7	0.06	0.20		
	Sn	0.60	9.6	1.73	1.5	1.3	1.5	0.6	0.19	0.00	No	No
	Ba	14.6	46.2	32.2	32.6	6.6	32.5	4.1	0.08	0.18		
	Pb	5.6	20.2	8.6	8.2	2.2	8.3	0.9	0.16	0.00	No	No
	THg	0.055	1.33	0.21	0.15	0.18	0.18	0.05	0.20	0.00	No	No

Note: Bulk sediment values (<125-mm sieved fraction, dry weight). Magnetic susceptibility (χlf) values, dimensionless. Organic content (LOI^{550}), Mg to Fe in % dry weight. Ni to THg in $\mu g \cdot g^{-1}$. Hubers (H_{15}) mean and median absolute deviation (MAD). KS, Kolmogorov–Smirnov non-parametric test; SW, Shapiro–Wilk test. Rejection of H_0 ($p < 0.05$).

using mean values from the SB soil core (Table 3). Deeper soil values from MG for background concentrations were not used due to occupation debris present in the whole sequence of materials at MG (Dunn & Mazzullo, 1993). Similarly, the use of the basal reef bedrock or sediments for background values was precluded due to their natural dissimilarity and biocarbonate composition.

Metal EFs are calculated using the following equation:

$$\text{EFelementX} = (X_{sample}/Al_{sample})/(X_{background}/Al_{background}), \quad (1)$$

where Al is a conservative, abundant and lithogenic element and dominant component of clay minerals and proxy of fine-grained sediment abundance. The effect of using different background values in the calculation is apparent (Table 3). Using mean SB core concentration as 'background' to calculate enrichment factors reduces EF values of P, Ni, Cu, Zn and THg in MG surface soils (compared with mean crustal concentrations) and illustrates the subjective use of 'background' in geochemical surveys (Reimann & de Caritat, 2005; Reimann et al., 2005).

$EF_{Crustal}$ THg values range from 2 to 65. EF_{SB} values are between 0.17 and 4.5 (Table 3). Outstanding $EF_{Crustal}$ and EF_{SB} values of THg at SF52 and SF76 indicate an anthropogenic or strong biological accumulative cause. Other trace metal EF values (excluding THg) at MG using mean crustal and SB values indicate little (EF < 1) or minor (EF < 3–5) enrichment (Table 3) with interspersed sample-specific 'hot-spots' (Figure 3). Samples SF18 and SF53 (EF_{SB}) in the high northern-central area are consistent with higher Pb and Sn. At SF14

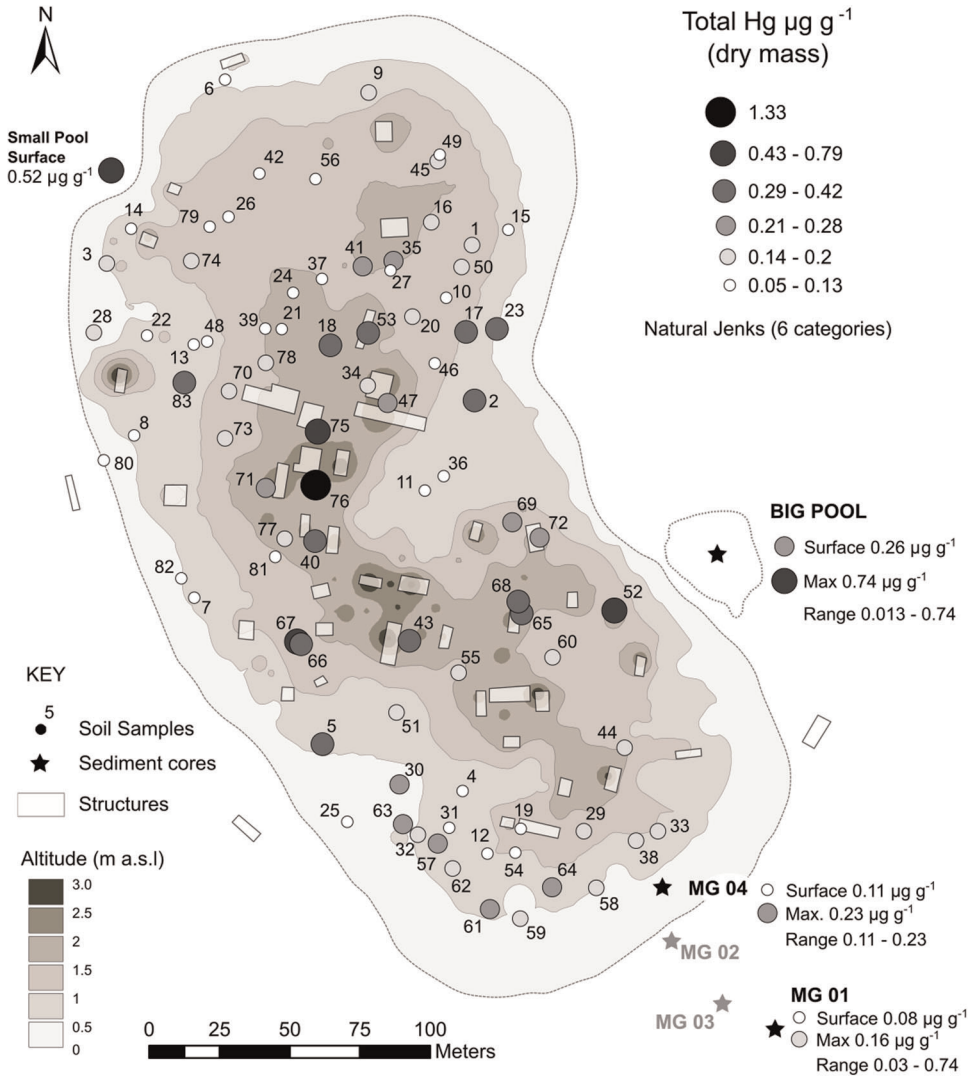

FIGURE 2 Total mercury (THg) in Marco Gonzalez (MG) soils. Surface and maximum concentration of THg in mangrove and pool sediments are also shown for comparison [Color figure can be viewed at wileyonlinelibrary.com]

near Structure 27, a high EF_{SB} for Zn, Cu and Pb occurs along with a cluster of elevated values in the southernmost area of the site, suggesting a broader area of metal enrichment.

Sampling points with enhanced EF_{SB} of THg, Cu, Sn and Pb also appear in box and whisker and covariate plots (Figures S2 and S10), as outlier values. Raising the outlier threshold of MG soil element concentrations to median +2 MAD for THg and Cu (and to an extent Zn) also emphasises the sample points SF52, SF67, SF75 and SF76 (Figure S11). The number and pattern of >2 MAD Zn values correspond with sites where ceramic/conch sherds are abundant at the sampling location (SF14), but also with leaf litter (SF76, SF77). Aside from Zn, the spatial patterns of >2 MAD values of trace metals largely correspond with the central, higher elevation area of the site.

On-site visibility of greater amount of leaf litter in the higher, more central area of MG during sample collection is reflected in the spatial results of LOI^{550} measurements (Figure S7) and correlation with altitude ($r = 0.715$) (Figure S9). Values of trace metals in bulk samples can be affected by concentration of organic matter, especially Hg, which is known to be sorptive to organic matter. The highest THg and LOI^{550} values were both found in the same soil sample (SF76); however, correlation values and covariate plots of LOI^{550} with THg indicate a non-direct relationship.

3.1.2 | Multivariate analysis: Geochemical spatial soil associations

Exploratory multivariate and spatial data analysis provides further confirmation of anomalous values and evidence of geochemical patterns related to position at the site. Element concentration maps (Figures S3–S7) indicate a high amount of spatial heterogeneity with scattered points of higher concentrations. Nonetheless, some broad spatial patterns are visible; the most obvious are higher concentrations of Sr occuring at lower elevations of the site while organic

TABLE 2 Mean element concentrations in MG surface soils (MG_{soils}), San Bar (SB) soils (mean of depths, 0–20 cm) and upper crust (UC) (Rudnick & Gao, 2003)

Element	MG_{soils} (*SD*)	SB	UC	Element	MG_{soils} (*SD*)	SB	UC
Mg %	2.2 (0.6)	1.8 (0.25)	1.5	Cu	23.9 (6.9)	1.2 (1.0)	28
Al %	2.9 (0.8)	0.5 (0.1)	8.1	Zn	63.5 (27)	3.0 (2.2)	67
Si %	5.7 (1.2)	1.6 (0.5)	31	As	17.2 (9.1)	2.1 (1.7)	4.8
P %	0.7 (0.3)	0.03 (0.01)	0.06	Br	206.5 (46.4)	168.1 (85.0)	1.6
K %	0.2 (0.1)	0.02 (0.03)	2.3	Rb	10 (2.1)	2.8 (1.1)	84
Ca %	23.7 (4.6)	35.8 (3.3)	2.5	Sr	2630 (583)	2095.1 (184.2)	320
Ti %	0.14 (0.03)	0.03 (0.01)	0.4	Y	13.4 (4.6)	2.0 (0.6)	21
Mn %	0.01 (0.00)	0.003 (0.001)	0.07	Zr	54.6 (12.3)	34 (8.5)	193
Fe %	0.9 (0.2)	0.13 (0.05)	5.8	Sn	1.7 (1.2)	1.7 (0.4)	2.1
V	53 (28)	nd	97	Ba	32.2 (6.6)	18.1 (7.2)	628
Cr	65 (24)	nd	92	Pb	8.5 (2.2)	4.4 (1.0)	17
Ni	15.7 (7.6)	3.1 (1.4)	47	THg	0.2 (0.18)	0.04 (0.01)	0.05

Note: Standard deviation (*SD*) values in brackets. Values in $\mu g \cdot g^{-1}$ except Mg to Fe (%).
Abbreviation: nd, not detected.

TABLE 3 Enrichment factor (EF) differences in Marco Gonzalez surface soils by using upper crust ($EF_{Crustal}$) (Rudnick & Gao, 2003) and San Bar (EF_{SB}) values of selected trace elements and Al

	$EF_{Crustal}$		EF_{SB}	
	Mean (*SD*)	Range	Mean (*SD*)	Range
THg	31.2 (25.8)	6.2–159.5	1.7 (1.4)	0.3–8.6
Ni	0.6 (0.2)	0.1–0.9	0.8 (0.3)	0.2–1.3
Cu	1.2 (0.4)	0.6–3.3	3.4 (1.2)	1.8–9.4
Zn	2.1 (1.3)	0.9–10.6	3.7 (2.2)	1.5–18.1
As	22.2 (8.3)	2.2–37.7	0.9 (0.4)	0.1–1.6
Sn	2.9 (1.9)	0.6–12.7	3.6 (2.3)	0.9–16.9
Pb	5.6 (1.3)	3.5–12.4	0.4 (0.1)	0.2–0.8

Abbreviation: THg, total mercury.

matter, magnetic susceptibility, Pb and THg values are notably higher in the central area of the site.

Principal component analysis (PCA) is useful in identifying multi-elemental geochemical associations by reducing a large number of variables to a small set retaining the information of the whole data set. The concentrations of all elements and values of LOI^{550} and χlf were used as input values for PCA. PCA analysis used a correlation matrix with values transformed to *z* scores. The first four PCA components explain 77.5% of the total variance. Axis 1 (Figure 4b) explains 49.6% of the variance, describing a spectrum dominated by negative loadings of Sr (−0.879) and Ca (−0.899) from carbonate bioclastic material, and positive loadings of lithogenic elements, that is, Al (0.95), Fe (0.97), Ti (0.92), Y(0.98) and Ni (0.94). The second axis (13.6% variance) relates to positive loadings of Cu (0.67), Zn (0.64), Hg (0.69), P (0.58) LOI^{550} (0.47) and χlf (0.59). PCA analysis of the multivariate element data describes a similarity between nearby samples and but also distance-separated samples with similar environmental conditions. Samples from the southern periphery of MG are geochemically distinct from the western, northern, and northwest peripheral sample points. Similarity between adjacent samples is highlighted in the samples from the high centre of the site around Structures 24, 29, 23 (SF47, SF75 and SF76) and Structure 34 (SF18) (see Figures 1 and 4a for locations). Outlier samples recognised previously are self-evident, extending positively from the second axis, including SF52 and SF76.

Cluster analysis was also conducted on the multivariate data set (Figure S12) that similarly identified the observed spatial and geochemical grouping from PCA analysis. The technique, incorporating a Euclidean distance measure in the algorithm, also picks out the similarity of close samples, that is, SF66 and SF67 that were collected as replicates from the same location, SF11 and SF36 from the floor of the central-eastern 'inlet' into the site (Figure 1) and SF4 and SF31 found close by in a dense sherd scatter in the south of the site. The outliers SF52 and SF76 are represented by the long length of the dendrogram arms (Figure S12).

3.1.3 | Spatial patterns of THg and trace metals due to structure and vegetation proximity

An increase of THg with proximity to structures is suggested by comparison of concentrations found in soil samples closest to mapped features (Figure 5). This may be expected if the source of mercury is due to its processing having occurred in production areas associated with specific buildings or domestic locations where

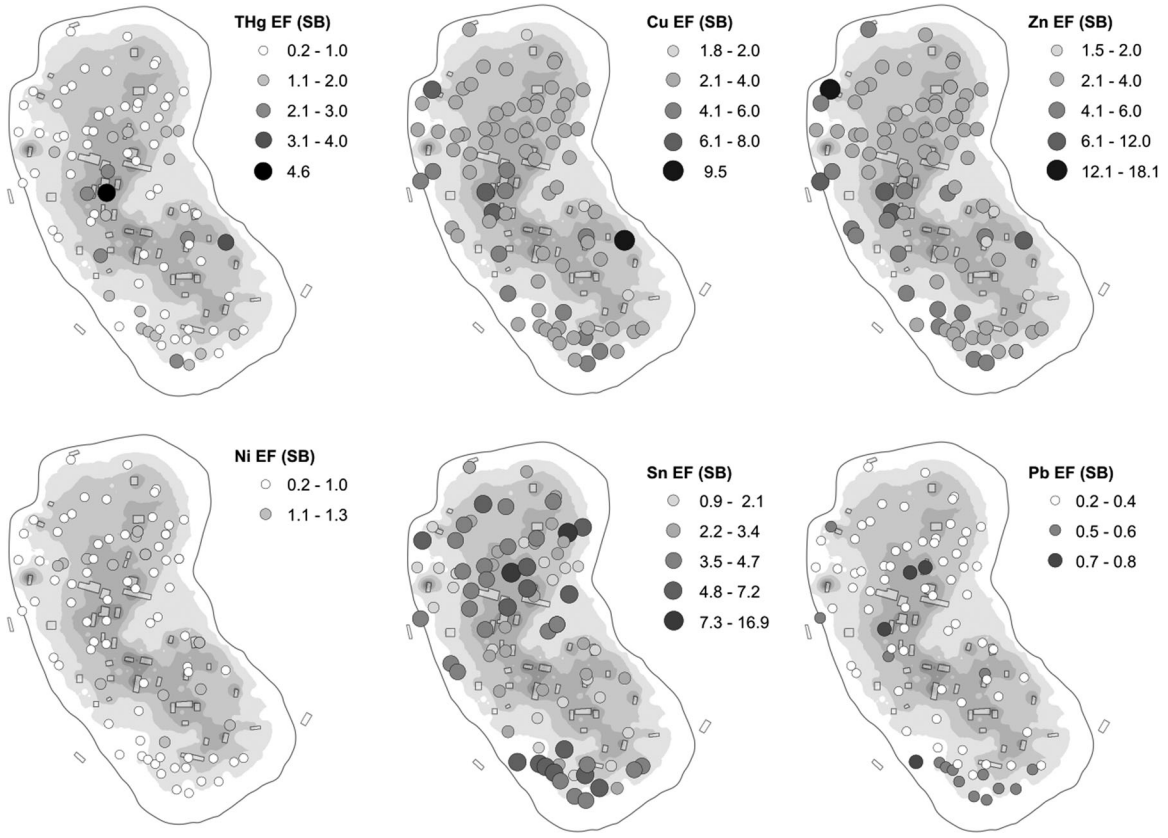

FIGURE 3 Enrichment factors (EF) of total mercury (THg) and trace metals in Marco Gonzalez (MG) soils using San Bar (SB) soil core values of trace metals and aluminium as background. See Figure 1 for locations, structures and ground surface altitude [Color figure can be viewed at wileyonlinelibrary.com]

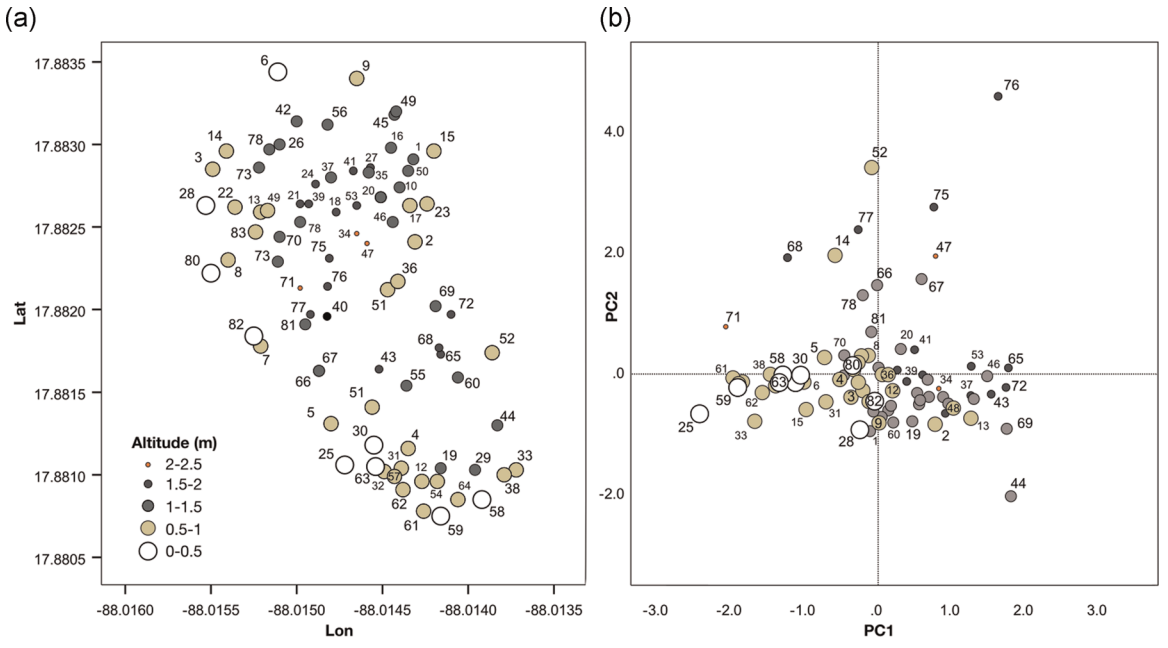

FIGURE 4 (a) Location and altitude of soil samples and (b) principal component analysis (PCA) output (PC1 and PC2 axes scores) of element abundances. Soil sample number labelled, and circles scaled by 0.5-m altitude buckets [Color figure can be viewed at wileyonlinelibrary.com]

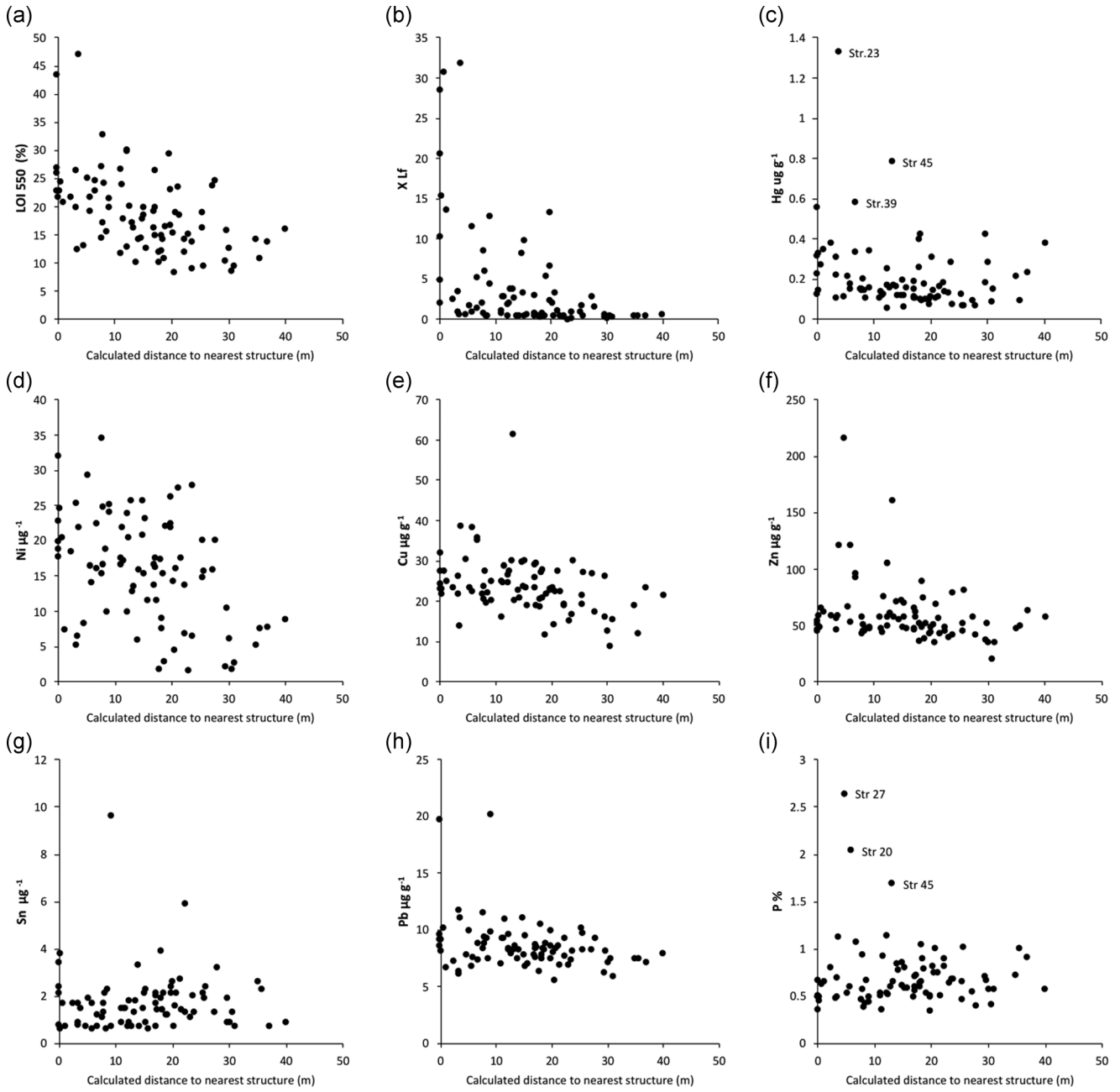

FIGURE 5 Element values measured against calculated distance from structures (a) LOI^{550}, (b) magnetic susceptibility, (c) total mercury, (d) nickel, (e) copper, (f) zinc, (g) tin, (h) lead and (i) phosphorus

mercury-containing products were used (Cook et al., 2006, 2017; Parnell et al., 2002). The four highest THg soil values are found within ~10 m of a structure (Structure 45 near SF52 is a wide platform area) but relatively high concentrations (~0.4 $\mu g \cdot g^{-1}$) are also found at greater distances from structures.

Zn, Cu and Pb have a comparable pattern with a few points of high concentration close to structures and a tailing-off of concentrations towards the site periphery. High χlf values also occur adjacent to structures and these may reflect greater amounts of occupation-altered soil and burnt ceramic waste in the samples. However, they may also be evidence of post-occupation bush-clearance fires or higher χlf due to bacterial magnetic enhancement in organic soils (Maher et al., 1999) that have developed around and on structure remains. The observed decrease of LOI^{550} with distance from structures is almost certainly autocorrelative, due to trees and structures occupying the centre of the site and accumulation of leaf litter-rich soil on top of and between structures. Preliminary results from comparison and mapping of THg and metal concentrations found in recent litterfall and the location of corresponding vegetation allude to a covariance of THg with the presence of *Eugenia* sp. trees (Figures S13 and S14), but more detailed soil and vegetation mapping and mercury measurements are clearly required.

3.2 | Sediment core results

Cores collected from the south of the site record a transition from shallow-marine to mangrove sedimentation. Processed conch and ceramic sherds are more abundant proximal to MG in biogenic carbonate muds and sands beneath mangrove peat, indicating contemporaneity of local pre-mangrove sedimentation with occupation and coastal resource use (Figures 6 and S15).

3.2.1 | Big Pool core sediment sequence and dating

The Big Pool core collected in 0.48-m water depth consists of light-grey (10YR 8/1) coralline/shelly sand/silt overlain by a dark brown (10YR 2/2) gyttja. The transition between 36 and 25 cm was noted during core extrusion as silty and increasingly organic mud. Ceramic sherds (<2 cm) and wood fragments were found in the organic mud, with shells of intact gastropods (*Hydrobia* sp.) visible in the upper 4 cm (Figures 6 and S15).

Total ^{210}Pb activity reaches equilibrium with the supported ^{210}Pb at around 12-cm depth. Unsupported ^{210}Pb activity, calculated by subtracting ^{226}Ra activity (as supported ^{210}Pb) from total ^{210}Pb activity, declines irregularly with depth (Figure S16). There is little net reduction in unsupported ^{210}Pb activity in the top 6-cm section with a maximum value at 4.5 cm, suggesting a gradual increase in sedimentation rates towards the sediment surface. From 6 cm downwards, unsupported ^{210}Pb activity declines irregularly but smoothly with depth, suggesting a gradual change in sedimentation rate. ^{137}Cs activity was not detectable in the sediments. Two very low measurements of the atmospheric nuclear testing isotope ^{241}Am are recorded at 2–3 and 11–12 cm. Without the detection of ^{137}Cs in the core, these are considered erroneous. ^{210}Pb chronologies were calculated using the constant rate of ^{210}Pb supply (CRS) model (Appleby et al., 1986).

SCPs are first detected in sediments from ca. 1960 AD (Figure 7). The first detection date resembles the SCP signal seen regionally in Central America from fossil-fuel power stations (Rose et al., unpublished data). Maximum concentration of SCPs occurs in sediments (5–6 cm) from 1980s. Conversion of SCP concentration to SCP accumulation rate (numbers cm^{-2}·year^{-1}) reveals a gradual decline in SCPs from 1970s to the present (Figure 7). A charcoal clast (2 cm) found at depth of 33–34 cm was ^{14}C-dated to 1568 ± 27 BP (AD 420–551 (2σ)). Compared with the age/depth of the peat transition in MG01 (and analyses of the surrounding sediment indicating an intertidal setting, below), this suggests the charcoal may have been washed in. A gradual transition rather than a hiatus or discontinuity is apparent in the elemental stratigraphy leading up to the early 20th century. Extending a linear sedimentation rate (0.32 mm·year^{-1}) below 10.5 cm suggests an estimated 11–12th century AD age for the carbonate sediment–mangrove transition in

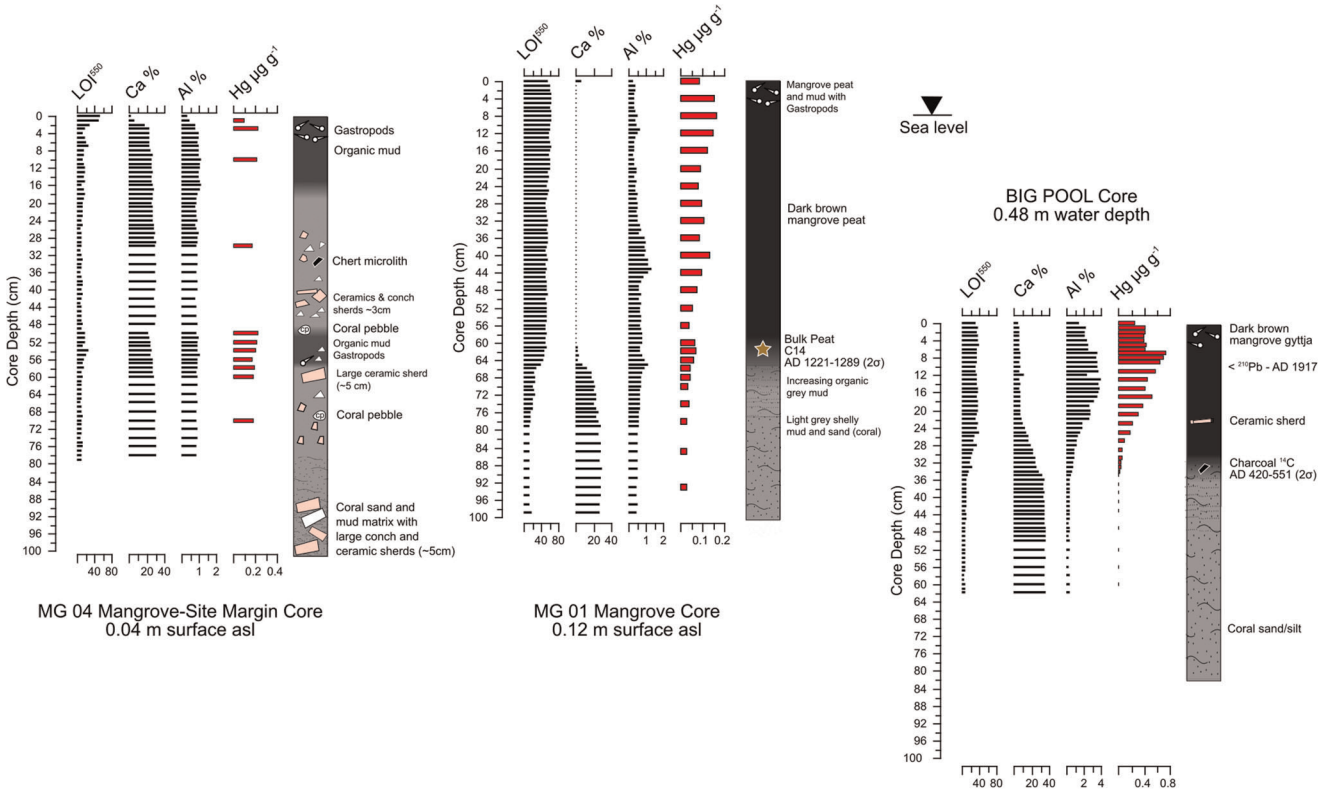

FIGURE 6 Mangrove (MG04, MG01) and Big Pool core stratigraphies of LOI^{550}, Ca%, Al% and total mercury (THg). MG04 and MG01 are spaced left to right in order of distance from Marco Gonzalez (MG). Vertical position of all cores to relative sea level (August 9, 2013). See Figure 1 for core locations [Color figure can be viewed at wileyonlinelibrary.com]

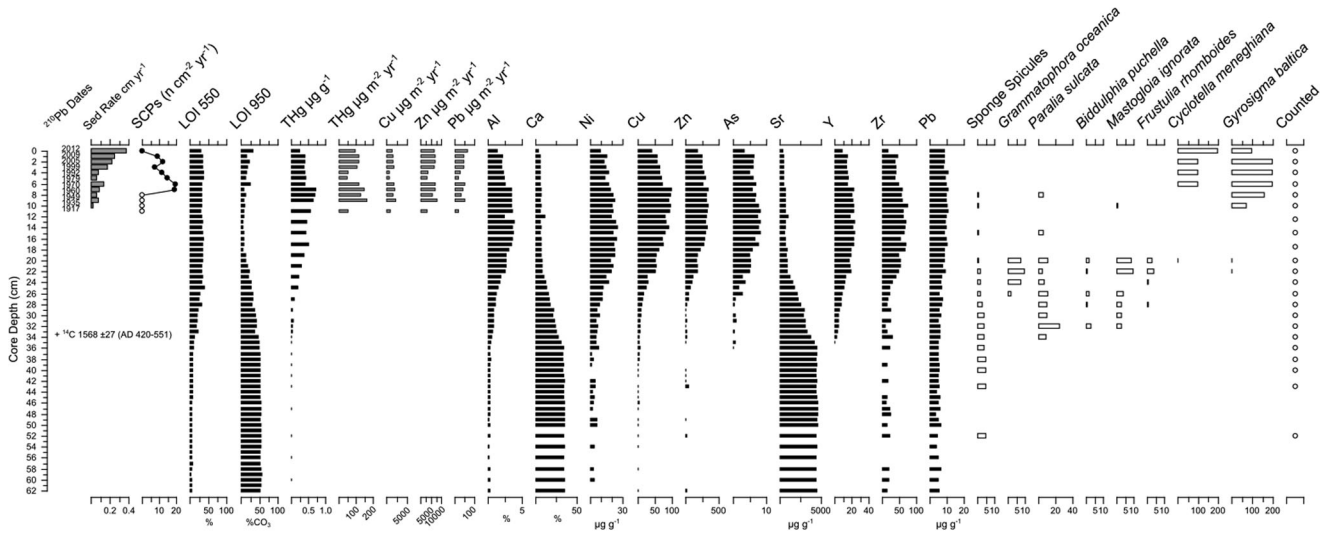

FIGURE 7 Big Pool stratigraphic summary of geochemical and diatom changes. ^{210}Pb calculated dates and sedimentation rates are shown. Depth and age of radiocarbon sample (UBA-27742) are shown. Unshaded circles indicate analysed but absent in sample. Total mercury (THg), Cu, Zn and Pb accumulation rates are calculated using ^{210}Pb sediment accumulation rate and element concentration data. See text for explanation of sponge spicule and diatom values

BP, which is comparable to the age of the basal peat in core MG01 (below).

3.2.2 | Big Pool core geochemical stratigraphy

The shift in the core between carbonate and organic/mineral sediment is very evident in the switchover of LOI^{950} and LOI^{550} values between 36 and 20 cm (Figure 7). This change is the shift of sediments dominated by Ca (and associated Sr) to organic sediment with allogenic elements (Si, Al, K, Ti, Fe, Mn, Rb and Zr) and trace metals (Ni, Cu, Zn, As, V, Cr and THg). THg values strongly correlate in the core with mineral element (Al) abundance (r^2 = 0.946, Ti, 0.958, p < 0.01) and trace metals (Zn, r^2 = 0.972, Cu, 0.987, p < 0.01) but also LOI^{550} (r^2 = 0.88, p < 0.01). THg concentrations are low in coral/shelly sand/silt (<0.03 µg·g^{-1} below 34 cm) and rise gradually to a peak concentration (0.741 µg·g^{-1}) at 7-cm depth (AD 1960 ± 7) (Figures 7 and S16). THg in sediments ^{210}Pb-dated (but SCP-absent, 8–11 cm) to the early 20th century ranges between 0.59 and 0.70 µg·g^{-1}. A decline in THg concentration occurs in sediments post-1970–1980 up to the present (upper 6 cm) that corresponds with decreased minerogenic elements (except Si) and an increase in organic, carbonate elements and calculated sedimentation rate. Surface (0–1 cm) THg concentration is 0.26 µg·g^{-1}.

THg EF_{SB} values (Figure 8) show a similar upcore increase from 36-cm depth with EF_{SB} 1–2 (2.3 max. at 7 cm). Co-trending THg, Cu and Zn EF_{SB} (>10) values indicate a significant above-San Bar background metal input (associated with Al input) into Big Pool. Increased EF_{SB} values of Pb and Sn (and other metals below 36 cm) reflect the low Al below 36 cm in the core due to the dominance of reef-carbonate sediment (Figures 7 and S16).

Calculated trace metals and THg flux values (µg·m^2·year^{-1}) reveal early to mid-20th century increasing inputs (up to the 1970s) and then a decline and lesser rate of accumulation to present (Figure 7). Calculated flux values of trace metals and THg reveal that early 20th century (ca. 1917) inputs are low. Due to the sites' relative remoteness, this pattern of 20th century increases of THg and metal fluxes, with SCPs undetected at first, before both metals and SCPs peak in the mid-20th century, is suggestive of being wholly a result of atmospheric transport and deposition. A pre-industrial, Maya-influenced input is, however, assured by the trace metal and geochemical profiles before ^{210}Pb-dated sediments. Comparable values in the Small Pool surface sample (THg 0.52 µg·g^{-1}; LOI^{550} 47.8%, Cu 39 µg·g^{-1}, Zn 412 µg·g^{-1}) (Figure 2) suggest that MG soil–mangrove interface habitats are critical in the landscape for the accumulation of trace metals.

3.2.3 | Big Pool core diatom changes

Diatom preservation in the core was poor with data collated as numbers of species identified per 10 transects of microscope slide (×400 magnification, 19-mm-diameter coverslip). Difficulty in counting was caused by a dense matrix of broken diatom and siliceous particles that was resistant to separation from identifiable valves with diluted samples. However, three broad ecological habitats are identified by the presence/absence of diatom and sponge spicule remains: below 35 cm, only fragments of sponge (*Placospongia* sp.) spicules were encountered, indicating a shallow-marine environment, between 35 and 15 cm, marine–brackish and brackish–fresh diatoms suggest intertidal to marine conditions and a final phase from the late 19th to early 20th century AD of a marine-disconnected, brackish pool (Figure 7).

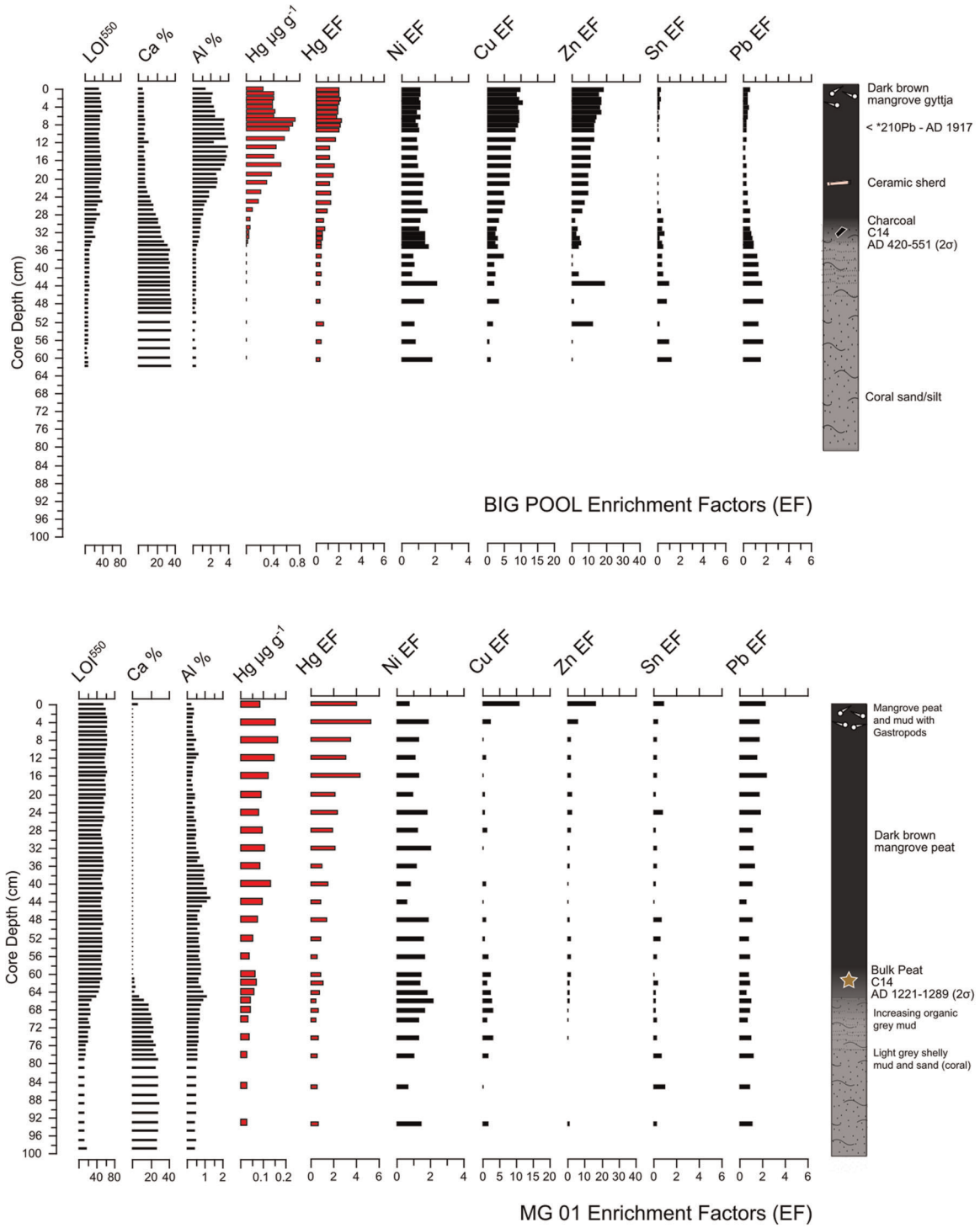

FIGURE 8 Enrichment factors (EF) calculated for Marco Gonzalez (MG) Big Pool (top) and MG01 (bottom) using San Bar background concentrations of Al and trace metals [Color figure can be viewed at wileyonlinelibrary.com]

3.2.4 | MG01 core dating and core geochemistry

The 1-m mangrove core consists of a light-grey (10YR 8/1) shelly sandy mud (below 80 cm) grading upwards into an increasingly organic mud (80–68 cm) and a homogenous dark brown (10YR 2/2) mangrove peat (68 cm surface) (Figure 6). The shift from carbonate to organic/minerogenic muds is apparent in the plots of LOI_{550} and element values (Figures 6 and S19). The ^{14}C date on bulk organic sediment from 62 to 63 cm indicates that this transition to mangrove peat occurred at the site in the 13th century AD (AD 1221–1289 2σ). This age/core depth indicates a peat accumulation rate of ~0.8–0.9 mm·year^{-1} to present, which is comparable to the rate of

Late Holocene sea-level rise (~1 mm·year^{-1}) calculated from mangrove peat sequences in the region (Mckee et al., 2007).

High concentrations of Ca, Sr and Zr below 80 cm in the sandy mud suggest an open reef-carbonate shoreline (Zr being present due to less resistant sediment minerals having been winnowed away in the high-energy environment). THg concentrations are low (<0.03 μg·g^{-1} below 70 cm) in the coral/shelly sand/silt but increase gradually up-core with some small peaks (0.07 μg·g^{-1} at 62 cm, 0.13 μg·g^{-1} at 40 cm and 0.16 μg·g^{-1} at 8 cm) (Figures 6 and S19). Surface concentration of THg at MG01 is 0.08 μg·g^{-1}. THg concentrations increase and show a positive correlation with organic content LOI^{550} and Mg, K, Br and Rb (r^2 = 0.79, 0.76, 0.97, 0.91 and 0.86, respectively). Unlike the BP core, the correlation of THg with Al, Si and Ti and trace metals (Ni, Cu, Zn and Pb) is negative or low (r^2 = −0.23, −0.5, −0.36, −0.32, −0.40, 0.2 and 0.37, respectively). THg EF_{SB} shows a gradual increase of EF_{SB} from <1 in the basal carbonate sandy mud to 5 in the surface mangrove peat (Figure 8). EF_{SB} of Cu is enhanced during the transition from carbonate sand and with Zn in the organic peat of the upper 4 cm. Pb is relatively stable in the core, with low EF_{SB} values similar to THg (Figure 8) and only increasing slightly in concentration with Si, Ti and Fe, indicating its association with mineral elements (Figure S19).

Enhanced phases of mineral element concentration (especially Al, Si, Ti and Fe) occur throughout mangrove peat accumulation (Figure S19), between 60 and 70 cm possibly during mangrove establishment (~13th century AD) and again at 45–35 cm (~15th–16th century AD). An increase in Zr in the latter interval perhaps indicates that the mangrove received sediments from nearby carbonate shorelines as well as minerogenic mud. The suggested timing and form of allogenic element profiles during peat accumulation allude perhaps to a record of a hurricane surge and mangrove recovery event, like the 'outstanding hurricane (Event 7) ca. 1500 AD' found in wetland sediments at Dangriga (100 km·S) (McCloskey & Keller, 2009) or perhaps a significant raft of pumice from Lesser Antillean eruptions (Carazzo et al., 2012; Roobol & Smith, 1980).

3.2.5 | Proximal core MG04 and mangrove MG02 and MG03 cores

Locations and altitudes/descriptions are presented in Figures 1 and S15. MG04 core consists of a light-grey (2.5Y 6/0) sandy mud with interspersed gravel and pebble-sized fragments of ceramic, conch and chert. Two phases of darkening and more organic composition were observed: between 58 and 50 cm and from 16 cm to the surface (Figure 6). Open-gouge corer penetration deeper than 88 cm was restricted by a waterlogged matrix of coral sand and mud with large (~5 cm) conch and ceramic sherds.

The low-organic and high-carbonate nature of MG04 sediments is apparent in the LOI^{550}, LOI^{950} and Ca and Sr downcore profiles, such that concentrations are comparable to the surface soils found along the southern margin of MG. The darkening phase of mud of 58–50 cm corresponds to a small increase in LOI^{550} (10%–11% at 62 cm, 30% at 55 cm and 12% at 48 cm) and increase again in the upper 10 cm (16% at 10 cm, 54% in the surface 1 cm). A concomitant drop in Ca and Sr occurs, as in MG01 when organic matter increases, along with some small increases in Cu, Zn and As (Figure S20). The co-increase of mineral elements and trace metals with LOI^{550} observed in Big Pool and MG01 cores is not obvious in MG04. Only in the upper 10 cm to the surface is a more pronounced increase in LOI^{550} with Cu, Zn, Sn and Br.

THg measurements focused on the section of 58–50 cm where increased THg (max. 0.23 μg·g^{-1} at 50 cm) occurs along with Cu, Zn and As (Figures 6 and S20). THg EF_{SB} values in MG04 are comparable to MG01, enhanced at (EF_{SB} 3) at 50 cm and EF_{SB} 3.8 in the topmost sample. Zn enrichment is far more enhanced, increasing to 6.9 at 50 cm but reaching an EF_{SB} of 30.3 in the surface sample due to high Zn and below SB soil Al concentrations.

The 50–58 cm depth phase in MG04 of darkening colour (10YR 3/1), LOI^{550} increase and mineral element changes are comparable to the depth of ~13th century AD peat establishment in MG01 (Figure 6) and therefore is proposed to be synchronous. Aside from the suggested phase of wetland formation, basal deposits (>88 cm) in MG04 from earlier Mayan occupation and afterwards, the core suggests a long-term accumulation of occupation waste into a non-mangrove coastal mud setting.

Intermediate cores (MG02, MG03) between MG04 and MG01 (Figure S15) reveal that MG occupation waste is mixed with pre-mangrove coastal sediments to at least 75 m south of the current mangrove edge of the site. Large (>10 cm) sherds and conch pieces occur in MG02 and MG03 in a saturated coral sand and mud matrix. The size and abundance suggest use, breakage and dumping nearby. In MG02, ceramics and conch fragments retain sharp fractures, indicating little evidence of transporting and post-disposal re-working. It is unclear if the clasts were dumped beneath the water of a sheltered, muddy shoreline or on a land surface with subsequent fine-grained intertidal mud and/or slope wash infilling over time.

Further coring is required to ascertain the spatial extent of these units, particularly whether the ~30-cm-thick deposit of conch and sherds in MG02 represents a single event (e.g., one period of salt making and conch preserving) or an accumulative feature over many years. Fragments in MG03 were less abundant at a similar depth (and age). If the thickness of occupation debris deposit translates to intensity of processing, we might assume that muddy, open shoreline conditions found between MG04 and MG02 core were the focus of such activities.

4 | DISCUSSION

4.1 | Elevated THg in MG anthropogenic-influenced soils

Concentrations of THg found in surface soils and archaeological contexts of MG are low as compared with deposits associated with Hg caches, burial practices or human remains alluding to chronic

TABLE 4 Concentrations of THg (and where co-measured) Cu and Zn in (a) Mayan archaeological and stratigraphic contexts, (b) other Central/South American mangrove coastal sediments and selected historical sediment records globally of mercury from artisan and industrial sources

Source	Location	Contexts	Hg values ($\mu g \cdot g^{-1}$)	Hg method and analysis
(a) Mayan contexts				
This study	MG, Belize	Surface soils ($n = 83$)	0.05–1.33	Total, AR, CVAFS
		Mangrove core (MG1) ($n = 25$)	0.03–0.17	Total, AR, CVAFS
		Mangrove core (MG4) ($n = 11$)	0.10–0.23	Total, AR, CVAFS
		Big Pool (BP) core ($n = 33$)	0.01–0.74	Total, AR, CVAFS
		Small Pool (surface mud sample)	0.52	Total, AR, CVAFS
		San Bar Caye soils ($n = 9$)	0.03–0.06	Total, AR, CVAFS
Macphail et al. (2016)	MG, Belize	Stratigraphic contexts ($n = 39$)	0.015–0.47	Total, AR, CVAFS
Battistel et al. (2018)	Peten Itza, Guatemala	Lake sediments	0.03–0.11	Total, AR, ICP-MS
Cook et al. (2006)	Cancuén, Guatemala	Soil floor deposits	0.04–0.99	Total, NR, ICP-MS
Fulton et al. (2017)	Palmarejo, Honduras	Plaza anthrosol (*sascab* plaster)	max. 3.4	Partial, AR, ICP-MS
Lamoureux-St-Hilaire et al., (2019)	La Corona, Guatemala	Palace plaster floors and overlaying soil matrices	max. 0.058	Partial, AR, ICP-MS
LeCount et al. (2016)	Actuncan, Belize	Palace plaster floors	max. 0.0016	Partial, AR, ICP-MS
Sills et al. (2016)	Chan b'i, Belize	Submerged peat (salt works)	max. 0.001	Partial, AR, ICP-MS
Wells et al. (2000)	Piedra Negras, Guatemala	Midden deposits THg near Hg cache	0.9–4.5 4.8	Partial, DTPA, ICP-OES
(b) Other contexts				
Acevedo-Figueroa et al. (2006)	Puerto Rico	San Jose Lagoon Joyuda Lagoon	0.1–4.9 0.1–0.3	Total, CVAFS
Benoit (2018)	St Thomas, USVI	Coastal pond sediments (20th C) Coastal pond sediments (19th C)	0.02–0.11 <0.04	Total, DMA Total, DMA
Guzmán and García (2002)	Panama	Modern coral	0.0214 ± 0.01	Total, AR, CV-AAS
		Coral sediments (surface)	0.062 ± 0.02	Total, AR-HF, CV-AAS
	Costa Rica	Modern coral	0.0152 ± 0.006	Total, AR, CV-AAS
		Coral sediments (surface)	0.086 ± 0.038	Total, AR-HF, CV-AAS
Rúa et al. (2014)	Darién Gulf, Colombia	Estuarine sediment	0.069–0.114	Total, DMA
Conrad and Sanders (2017)	Paranagua Bay, SE Brazil	Mangrove sediment Pre-AD 1900 and Modern	<0.03	Total, AR, CVAFS
Machado et al. (2002)	Guanabara Bay, Brazil	Mangrove (100 m from landfill)	0.27–0.89	Total, AR, CVAFS
		Mangrove (degraded)	0.26–0.35	Total, AR, CVAFS
Silva et al. (2003)	Sepetiba Bay, Brazil	Mangrove forest	0.02–0.06	Total, AR, CVAFS
		Tidal creek	0.05–0.09	Total, AR, CVAFS
		Mud flat	0.05–0.18	Total, AR, CVAFS
Elbaz-Poulichet et al. (2011)	Pierre Blanche Lagoon, France	Mud AD 1945–1968 Mud AD 1650 Mud AD 1150 Mud prior AD 900	0.58 0.082 0.13 0.017	Total, DMA

TABLE 4 (Continued)

Source	Location	Contexts	Hg values ($\mu g \cdot g^{-1}$)	Hg method and analysis
Fitzgerald et al. (2018)	Pettaquamscutt Estuary, RI, USA	Mud AD ca. 1996 Mud AD 1950–1975 Mud AD 1830–1901 Background	<0.15 ~0.35 <0.2 ~0.05	Total, DMA
Laperche et al. (2014)	Amazonian river muds, French Guiana	Gold mining areas Close to mined sites Low-Hg river mud Estuarine mud	<0.5–50 >0.2 <0.15 <0.06	Total, DMA (and CVAFS)
Rood et al. (1995)	Florida Everglades, USA	Wetland soils—post-AD 1985 Wetland soils—ca. AD 1900	0.01–0.48 0.01–0.14	Total, AR, CVAFS
Wang et al. (2018)	Pearl River, China	Estuarine mud (recent)	0.03–0.39	Total, AR, CVAFS

Abbreviations: AR, aqua regia digestion; AR-HF, aqua regia and hydrofluoric acid digestion; CV-AAS, cold vapour atomic absorption spectroscopy; CVAFS, cold vapour atomic fluorescence spectroscopy; DMA, direct (pyrolytic) mercury analyser; DTPA, diethylenetriaminepentaacetic acid; ICP-MS, inductively coupled plasma mass spectrometry; ICP-OES, inductively coupled plasma optical emission spectroscopy; MG, Marco Gonzalez; NR, nitric acid digestion; Partial, partial extraction digestion (not total mercury); Total, total mercury.

mercury exposure (Batta et al., 2013; Emslie et al., 2015; Wells et al., 2000). Direct comparison of values found in MG soils with other published Mayan contexts is problematic by the wide use of partial-extraction analyses (Table 4a). The highest values of THg at MG are, however, comparable to those measured using total extraction and abundance in Mayan floor deposits with evidence of cinnabar use (Table 4a). At Cancuén, Guatemala, a THg hot spot of 1 $\mu g \cdot g^{-1}$ was measured in the soil at the southern edge of a burial that contained two ceramic offerings which may also have contained cinnabar (Cook et al., 2006).

Although the second and third highest THg values (SF52, SF67, 0.79, 0.58 $\mu g \cdot g^{-1}$, respectively) were measured where occupation waste (sherds, obsidian, fish vertebrae and charcoal) was recorded on the land surface, the first and fourth ranked values (SF76, SF75, 1.3, 0.5 $\mu g \cdot g^{-1}$, respectively) occur in leaf litter-rich soils. This dichotomy emphasises the requirement to understand the broader spatial and contextual pattern of Hg in anthropogenic soils before solely attributing its presence to human activity. These points of higher concentration merit future investigation to look for cinnabar, Hg-pigmented materials or other metalliferous waste, as the clear co-enrichment with Cu and Zn at SF52 (Figure 3) suggests a mixed source of trace metal-elevated materials.

Despite the relatively low THg values measured in deep stratigraphic contexts, near-surface THg values at MG may be elevated due to bioturbation and other mechanisms of vertical mixing bringing to the surface a more inclusive sample of below-ground materials. Assimilation and mixing of subsurface contexts are evident at MG from the abundance of land crab (*Cardisoma guanhumi*) burrows and carapace remains. Burrow entrances are marked by a fan of mud often containing ceramics, conch shell and other subsurface-derived materials. *C. guanhumi* burrows extend often down to the water table and can occur in densities >1 burrow per m^2 (Gifford, 1962). Excavation of burrows on-site have revealed the considerable vertical and lateral extent of crab burrows (Glanville-Wallis, 2015), yet also that bioturbation has not been total, especially in the higher, central section of the site where the water table is too deep. Similar vertical mixing from tree-root throw, other organisms, historical looters pits and excavation waste must also be considered. Considering the evidence of significant enhancement of THg and other trace metals in adjacent mangrove pool and peat sediments, the incorporation of off-site muds also cannot be ruled out, that is, from hurricane washover events. The resolution and detail of sampling and analysis used in this study preclude a definite causation of hot spots that will be assessed using more detailed spatial pedological surveys at MG.

4.2 | Hg sources and cycling at MG

Soil patterns of elevated THg in organic matrices and fine-grained allogenic materials are evident in core sediments of MG01 and BP. Enhanced THg owing to predominantly minerogenic inputs is also apparent in MG04. Synchronous fine-grained and organic sediment accumulation is characteristic of coastal mangrove and mudflat development, so a coincidental increase in THg and other trace elements is not unexpected.

A local MG source and process of Hg accumulation are suggested, not just from the discovery of points of elevated concentrations but also by overall concentrations exceeding mean crustal concentrations of THg (0.05 $\mu g \cdot g^{-1}$) also found in the 'background' SB core. THg concentrations in MG wetland samples are greater than sediment concentrations found in mangrove margins of contemporary urban waste dumps in Brazil (Machado et al., 2002; Silva et al., 2003) and tropical coastal lagoons receiving urban runoff (Acevedo-Figueroa et al., 2006; Conrad & Sanders, 2017) (Table 4b). Similarly, THg values in sediment cores from MG are comparable and higher than THg measured in wetland, estuarine–lagoon muds linked to atmospheric deposition and waste from historical industrial and artisanal sources (Benoit, 2018; Conrad & Sanders, 2017;

Elbaz-Poulichet et al., 2011; Fitzgerald et al., 2018; Laperche et al., 2014; Rood et al., 1995; Wang et al., 2018) (Table 4). With regards trace metal waste, MG might be considered to have acted as a leaky landfill during and post-occupation, contributing to long-term legacy contamination of surrounding coastal wetland habitats.

Concentrations of THg (and other trace metals) in mangrove, pool core, stratigraphic contexts and topsoil samples at MG largely increase (with clear non-outliers) with the abundance of organic matter and aluminium (fine-grained allogenic) sediment (Figure 9). With both, however, comes the potential of non-anthropogenic biogeochemical processes (i.e., mangrove soil development, redox changes, leaf litter accumulation and plant and organism movement) having influenced the temporal and spatial patterns.

Accumulation of mercury clearly started with the shift away from Ca–Sr (carbonate)-rich deposition. In MGO1, replacement of Ca–Sr carbonate sediment with mineral sediment and mangrove-enhanced THg concentration occurred in Big Pool at the earliest, post-6th century AD, in MG01 from the 13th century AD. In MG04, assuming that ~65 cm depth in the core is analogous to the organic shift in MG01, THg concentration has remained high (ca. 0.3 $\mu g \cdot g^{-1}$) in post-13th century AD sediments with relatively stable, carbonate, organic matter and mineral element patterns. Continued above-background THg concentrations in MG04, plus its proximity to MG, suggest it has been sourced from the site and transported to MG04.

Although core data indicate time-consistent occupation and Hg accumulation, the effect of biogeochemical cycling of Hg from the atmosphere, through vegetation, organisms and accumulation in soils cannot be overlooked. Organic cycling and bacteria perform a critical role in reduction, methylation and accumulation of mercury in sediments and soils. Physical and ecological conditions that lead to differential soil organic matter accumulation patterns also lead to differential Hg accumulation at a landscape scale (Grigal, 2003). Three significant biological processes of Hg cycling operate in close proximity at MG: mangrove peat formation, tropical forest litterfall and coastal food-web bioaccumulation.

Waterlogged mangrove soils provide conditions for both organic matter preservation and production of Hg, through low rates of decomposition, bacterial activity and complex root–sediment geochemical interactions transforming and exporting methylmercury (MeHg) (de Oliveira et al., 2015; Silva et al., 2003). The Small Pool surface sample collected at the MG site–mangrove margin (Figures 2 and S21) is where mangrove roots, saturated soil conditions, leaf litter and a mat of purple sulphur bacteria combine. This represents conditions that are likely to have been persistent and conducive to Hg accumulation in the intertidal zone surrounding MG throughout occupation and mangrove development.

Atmospheric capture, soil uptake and litterfall are also believed to be a major flux of Hg to forest soils; for example, in Brazilian coastal forests, leaves from the most abundant species contain 0.06–0.21 Hg $\mu g \cdot g^{-1}$ (Teixeira et al., 2012). The potential connection between *Eugenia* trees and elevated soil Hg needs to be explored further from the preliminary range of Hg values measured in soils, leaves and the spatial distribution of the tree species (Figures S13 and S14). Preferential leaf litter accumulation at MG is certainly to have been afforded by feedback in edaphic conditions, that is, a pocket of coastal forest developing on a coral caye (due to ground raising, anthrosol soils) and subsequent leaf litter allowed to accumulate in the irregular terrain created by structures. Enhanced THg concentrations within forest soils can occur due to decomposition of leaf litter, with Hg compounds (e.g., MeHg) transformed, recycled and retained in the upper organic horizons rather than moved down profile (Demers et al., 2007). Evidence of Hg being naturally enhanced in coral, mangrove and tropical woodland ecosystems, therefore, has significant implications in using Hg at coastal Mayan

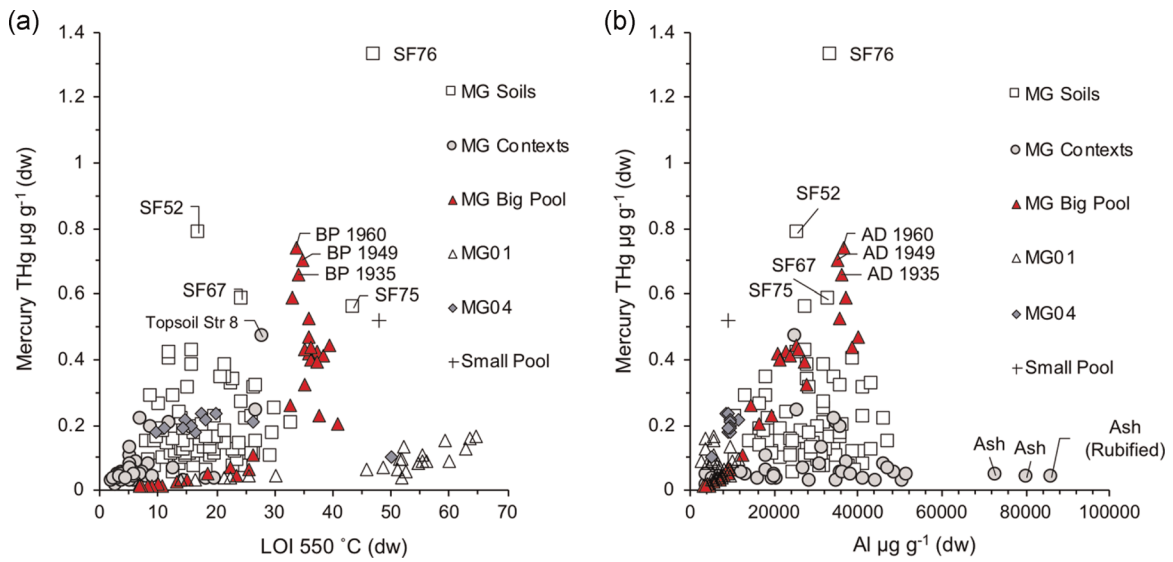

FIGURE 9 (a) Total mercury (THg) and LOI^{550} and (b) THg and Al $\mu g \cdot g^{-1}$ plot of Marco Gonzalez (MG) surface soil samples, MG stratigraphic contexts (Macphail et al., 2016), sediment cores and Small Pool sample. Ages of maximum THg in Big Pool and MG soil sample codes are labelled. High-Al containing ash samples were excavated on site of Structure 14 [Color figure can be viewed at wileyonlinelibrary.com]

sites to identify implicitly past utilisation and to what extent modern soil/sediment concentrations relate to archaeological remains or post-occupation ecosystem and soil development.

Another hypothesis is that along with human and sediment-imported Hg sources, the site during occupation operated as a centre of Hg biomagnification due to intensive resource use of coastal food webs. The large volume and type (large predatory fish, conch and manatee) of marine resources utilised by the Mayan population (Graham, 1994; Williams et al., 2009) through consumption of reef biota (M. F. M. Costa et al., 2012; Evers et al., 2009) could have made the site a pre-industrial source of Hg to local soils and wetland sediments.

The local absence of suitable sediments on Ambergris Caye for Mayan ceramic production and the identification of imported ceramic ware and lithic fragments found at MG suggest that natural mineral transport rates took a short-cut to MG via Mayan trade. Another consideration that will require further sedimentological and geochemical evidence is to what extent volcanic materials, in the form of pumice, in particular, may have contributed to the lithogenic component of foreshore sediments at MG. Pumice is regularly found in modern beach deposits and within the mangrove from tidal and wave transport. Pumice occurs at low frequencies in MG archaeological deposits and pumice rings thought to been used as floats have been found in coastal Mayan middens in Belize (McKillop, 1984). Rafts of pumice from Lesser Antillean volcanic activity will have entered the coastal zone during occupation and post-occupation mangrove growth, with their breakdown products becoming potentially a significant minerogenic input into coastal peats. Manufactured ceramic waste, shell matter and other imported materials discarded in the intertidal zone must have influenced or even determined local sedimentation patterns and mangrove colonisation during and post-occupation of the MG site.

5 | CONCLUSION

Elevated sediment THg concentrations in organic soil and sediment matrices, plus their occurrence with occupation waste and other metal element signatures of human activity, suggest an historical anthropogenic-influenced process of mercury transport to MG. Trace metal enrichment of other metals (Cu, Zn, Ni and Pb) is slight, likely due to the low use of metals by the Maya and the sites' subsequent abandonment/distance from industrial contamination up to the present day. The dichotomy of THg hot spots—on the one hand, associated with occupation detritus and ceramics, and on the other, in association with organic and fine-grained lithogenic materials—indicates a complex pattern that will require focused surveying and future matrix-specific analytical techniques.

Modern soil and wetland formation at the site of MG has been a dynamic process of natural and human actions, combining late-Holocene development of a coastal coral caye and barrier complex, ground raising from structure construction and waste accumulation from Maya occupation and then post-occupation ecological and geomorphological changes. Isolating the causes of soil geochemical variability and determining the influence of human activity are difficult, even at an isolated site like MG where the composition of contemporary soils and morphology of the landscape have been clearly altered by human occupation. A larger investigation of mercury occurrence in coastal Belize is called for, at natural/undisturbed sites (like San Bar) and known Mayan/historical coastal archaeological sites that have had similar occupation/post-occupation trajectories of landscape and vegetation evolution. Similarly, comparison with inland Mayan sites is also required to test the extent of coastal resource utilisation on mercury accumulation and whether elevated mercury in anthrosols and sediments is a common archaeological signature of Mayan occupation and intensive use of coastal resources. Taking this and other studies forward, there is a clear rationale for standardising the collection, measurement and analysis of mercury in Mayan sediment and soil samples to understand its complex and long-term natural–human–geological interactions.

ACKNOWLEDGEMENTS

This study was funded by a Leverhulme Trust Research Project Grant 'The role of past human activity in structuring modern landscapes and soils'. PI: Elizabeth Graham, UCL, 2013. The authors are indebted to Jan Brown, Chairman of the Board of the Marco Gonzalez Maya Site, Ambergris Caye, Ltd., Preservation Group, for all her efforts on their behalf. They thank Eduardo Barrientos and Denver Cayetano from the University of Belize and Dr. Elma Kaye, Terrestrial Science Director of the Environmental Research Institute, for their invaluable assistance, and Jerry Choco for excellent site management.

CONFLICT OF INTERESTS

The authors declare that there are no conflict of interests.

REFERENCES

Acevedo-Figueroa, D., Jiménez, B. D., & Rodríguez-Sierra, C. J. (2006). Trace metals in sediments of two estuarine lagoons from Puerto Rico. *Environmental Pollution*, *141*(2), 336–342. https://doi.org/10.1016/j.envpol.2005.08.037

Adomat, F., & Gischler, E. (2015). Sedimentary patterns and evolution of coastal environments during the Holocene in central Belize, Central America. *Journal of Coastal Research*, *31*(4), 802–826.

Ander, E. L., Johnson, C. C., Cave, M. R., Palumbo-Roe, B., Nathanail, C. P., & Lark, R. M. (2013). Methodology for the determination of normal background concentrations of contaminants in English soil. *Science of the Total Environment*, *454–455*, 604–618. https://doi.org/10.1016/j.scitotenv.2013.03.005

Appleby, P. G., Nolan, P. J., Gifford, D. W., Godfrey, M. J., Oldfield, F., Anderson, N. J., & Battarbee, R. W. (1986). ^{210}Pb by low background gamma counting. *Hydrobiologia*, *143*, 21–27.

Appleby, P. G., Richardson, N., & Nolan, P. J. (1992). Self-absorption corrections for well-type germanium detectors. *Nuclear Instruments and Methods in Physics Research Section B*, *71*(2), 228–233. https://doi.org/10.1016/0168-583X(92)95328-O

Ávila, A., Mansilla, J., Bosch, P., & Pijoan, C. (2014). Cinnabar in Mesoamerica: Poisoning or mortuary ritual? *Journal of Archaeological Science*, *49*, 48–56. https://doi.org/10.1016/j.jas.2014.04.024

Batta, E., Argáez, C., Mansilla, J., Pijoan, C., & Bosch, P. (2013). On yellow and red pigmented bones found in Mayan burials of Jaina. *Journal of Archaeological Science*, *40*(1), 712–722. https://doi.org/10.1016/j.jas.2012.08.013

Bell, E. E. (2007). Early Classic ritual deposits within the Copan acropolis: The material foundations of political power at a Classic period Maya center. University of Pennsylvania. https://repository.upenn.edu/dissertations/AAI3260880

Benoit, G. (2018). Mercury in dated sediment cores from coastal ponds of St Thomas, USVI. *Marine Pollution Bulletin*, *126*, 535–539. https://doi.org/10.1016/j.marpolbul.2017.09.056

Carazzo, G., Tait, S., Kaminski, E., & Gardner, J. E. (2012). The recent Plinian explosive activity of Mt. Pelée volcano (Lesser Antilles): The P1 AD 1300 eruption. *Bulletin of Volcanology*, *74*(9), 2187–2203. https://doi.org/10.1007/s00445-012-0655-4

Conrad, S., & Sanders, C. (2017). Influence of anthropogenic activities on trace metal accumulation in Brazilian mangrove sediments. Revista Virtual de Quimica. https://doi.org/10.21577/1984-6835.20170120

Cook, D. E., Beach, T., & Demarest, A. A. (2017). Soil and slaughter: A geoarchaeological record of the ancient Maya from Cancuén, Guatemala. *Journal of Archaeological Science: Reports*, *15*, 330–343. https://doi.org/10.1016/j.jasrep.2017.08.005

Cook, D. E., Kovacevich, B., Beach, T., & Bishop, R. (2006). Deciphering the inorganic chemical record of ancient human activity using ICP-MS: A reconnaissance study of late Classic soil floors at Cancuén, Guatemala. *Journal of Archaeological Science*, *33*(5), 628–640. https://doi.org/10.1016/j.jas.2005.09.019

Costa, B., Soares, T., Torres, R., & Lacerda, L. (2013). Mercury distribution in a mangrove tidal creek affected by intensive shrimp farming. *Bulletin of Environmental Contamination and Toxicology*, *90*(5), 537–541. https://doi.org/10.1007/s00128-012-0957-4

Costa, M. F. M., Landing, W. M., Kehrig, H. A., Barletta, M., Holmes, C. D., Barrocas, P. R. G., Evers, D. C., Buck, D. G., Claudia Vasconcellos, A., Hacon, S. S., Moreira, J. C., & Malm, O. (2012). Mercury in tropical and subtropical coastal environments. *Environmental Research*, *119*, 88–100. https://doi.org/10.1016/j.envres.2012.07.008

Cotin, J., García-Tarrasón, M., Sanpera, C., Jover, L., & Ruiz, X. (2011). Sea, freshwater or saltpans? Foraging ecology of terns to assess mercury inputs in a wetland landscape: The Ebro Delta. *Estuarine, Coastal and Shelf Science*, *92*(1), 188–194. https://doi.org/10.1016/j.ecss.2010.12.024

de Oliveira, D. C. M., Correia, R. R. S., Marinho, C. C., & Guimarães, J. R. D. (2015). Mercury methylation in sediments of a Brazilian mangrove under different vegetation covers and salinities. *Chemosphere*, *127*, 214–221. https://doi.org/10.1016/j.chemosphere.2015.02.009

Dean, W. E., Jr. (1974). Determination of carbonate and organic matter in calcareous sediments and sedimentary rocks by loss on ignition: Comparison with other methods. *Journal of Sedimentary Research*, *44*(1), 242–248.

Demers, J. D., Driscoll, C. T., Fahey, T. J., & Yavitt, J. B. (2007). Mercury cycling in litter and soil in different forest types in the Adirondack region, New York, USA. *Ecological Applications*, *17*(5), 1341–1351. https://doi.org/10.1890/06-1697.1

Denommee, K. C., Bentley, S. J., & Droxler, A. W. (2014). Climatic controls on hurricane patterns: A 1200-y near-annual record from Lighthouse Reef, Belize. *Scientific Reports*, *4*, 3876. https://doi.org/10.1038/srep03876

Desianti, N., Enache, M. D., Griffiths, M., Biskup, K., Degen, A., DaSilva, M., Millemann, D., Lippincott, L., Watson, E., Gray, A., Nikitina, D., & Potapova, M. (2019). The potential and limitations of diatoms as environmental indicators in mid-Atlantic Coastal Wetlands. *Estuaries and Coasts*, *42*(6), 1440–1458. https://doi.org/10.1007/s12237-019-00603-4

Desianti, N., Potapova, M., Enache, M., Belton, T. J., Velinsky, D. J., Thomas, R., & Mead, J. (2017). Sediment diatoms as environmental indicators in New Jersey Coastal Lagoons. *Journal of Coastal Research*, *78*, 127–140. https://doi.org/10.2112/SI78-011.1

Duncan, L. M. (2019). Archaeological deposits, environmental impact and local soil formation at Marco Gonzalez, Belize. UCL.

Dunn, R. K., & Mazzullo, S. J. (1993). Holocene paleocoastal reconstruction and its relationship to Marco Gonzalez, Ambergris Caye, Belize. *Journal of Field Archaeology*, *20*(2), 121–131. https://doi.org/10.1179/009346993791549183

Ebanks, W. J., Jr. (1975). Holocene carbonate sedimentation and diagenesis, Ambergris Cay, Belize. In K. F. Wantland & W. C. Pusey (Eds.), *Belize shelf—Carbonate sediments, clastic sediments, and ecology* (Vol. 2, pp. 234–296). American Association of Petroleum Geologists Studies in Geology.

Eberl, M., Alvarez, M., & Terry, R. E. (2012). Chemical signatures of middens at a Late Classic Maya residential complex, Guatemala. *Geoarchaeology-an International Journal*, *27*(5), 426–440. https://doi.org/10.1002/gea.21415

Elbaz-Poulichet, F., Dezileau, L., Freydier, R., Cossa, D., & Sabatier, P. (2011). A 3500-year record of Hg and Pb contamination in a Mediterranean sedimentary archive (The Pierre Blanche Lagoon, France). *Environmental Science and Technology*, *45*(20), 8642–8647. https://doi.org/10.1021/es2004599

Emslie, S. D., Brasso, R., Patterson, W. P., Valera, A. C., McKenzie, A., Silva, A. M., Gleason, J. D., & Blum, J. D. (2015). Chronic mercury exposure in Late Neolithic/Chalcolithic populations in Portugal from the cultural use of cinnabar. *Scientific Reports*, *5*, 14679. https://doi.org/10.1038/srep14679

Entwistle, J. A., Abrahams, P. W., & Dodgshon, R. A. (1998). Multi-element analysis of soils from Scottish historical sites. Interpreting land-use history through the physical and geochemical analysis of soil. *Journal of Archaeological Science*, *25*(1), 53–68. https://doi.org/10.1006/jasc.1997.0199

Evers, D. C., Graham, R. T., Perkins, C. R., Michener, R., & Divoll, T. (2009). Mercury concentrations in the goliath grouper of Belize: An anthropogenic stressor of concern. *Endangered Species Research*, *7*(3), 249–256. https://doi.org/10.3354/esr00158

Fitzgerald, W. F., Engstrom, D. R., Hammerschmidt, C. R., Lamborg, C. H., Balcom, P. H., Lima-Braun, A. L., Bothner, M. H., & Reddy, C. M. (2018). Global and local sources of mercury deposition in coastal New England reconstructed from a multiproxy, high-resolution, estuarine sediment record. *Environmental Science and Technology*, *52*(14), 7614–7620. https://doi.org/10.1021/acs.est.7b06122

Fordyce, F. M., O'Donnell, K. E., Lister, T. R., Breward, N., Johnson, C. C., Brown, S. E., Ander, E. L., & Rawlins, B. G. (2005). GSUE: Urban geochemical mapping in Great Britain. *Geochemistry: Exploration, Environment, Analysis*, *5*(4), 325–336.

Fulton, K., Wells, E. C., & Storer, D. (2017). Ritual or residential? An integrated approach to geochemical prospection for understanding the use of plaza spaces at Palmarejo, Honduras. *Archaeological and Anthropological Sciences*, *9*, 1059–1076. https://doi.org/10.1007/s12520-013-0170-3

Gan, H., Lin, J., Liang, K., & Xia, Z. (2013). Selected trace metals (As, Cd and Hg) distribution and contamination in the coastal wetland sediment of the northern Beibu Gulf, South China Sea. *Marine Pollution Bulletin*, *66*(1–2), 252–258. https://doi.org/10.1016/j.marpolbul.2012.09.020

Gifford, C. A. (1962). Some observations on the general biology of the land crab, *Cardisoma guanhumi* (Latreille) in South Florida. *Biological Bulletin*, *123*(1), 207–223. https://doi.org/10.2307/1539516

Gischler, E., & Hudson, J. H. (2004). Holocene development of the Belize barrier reef. *Sedimentary Geology*, *164*(3), 223–236.

Gischler, E., Shinn, E. A., Oschmann, W., Fiebig, J., & Buster, N. A. (2008). A 1500-year Holocene Caribbean climate archive from the Blue Hole, Lighthouse reef, Belize. *Journal of Coastal Research*, *24*(6), 1495–1505.

Glanville-Wallis, F. (2015). *'Of Crabs and Men': Artefact analysis of residual waste deposits; and a preliminary investigation into crab bioturbation at Marco Gonzalez; Belize* (Unpublished BSc Dissertation).

Golden, N., Morrison, L., Gibson, P. J., Potito, A. P., & Zhang, C. S. (2015). Spatial patterns of metal contamination and magnetic susceptibility of soils at an urban bonfire site. *Applied Geochemistry*, *52*, 86–96. https://doi.org/10.1016/j.apgeochem.2014.11.004

Graham, E. (1994). The Highlands of the Lowlands: environment and archaeology in the Stann Creek district, Belize, central America. In J. J. MacKinnon (Ed.), *Monographs in world archaeology*. Issue 19 (p. 372). Prehistory Press.

Graham, E., Macphail, R., Turner, S., Crowther, J., Stegemann, J., Arroyo-Kalin, M., Duncan, L., Whittet, R., Rosique, C., & Austin, P. (2017). The Marco Gonzalez Maya site, Ambergris Caye, Belize: Assessing the impact of human activities by examining diachronic processes at the local scale. *Quaternary International*, *437*, 115–142. https://doi.org/10.1016/j.quaint.2015.08.079

Graham, E., & Pendergast, D. (1989). Excavations at the Marco Gonzalez site, ambergris cay, Belize, 1986. *Journal of Field Archaeology*, *16*(1), 1–16. https://doi.org/10.1179/jfa.1989.16.1.1

Graham, E., & Simmons, S. (2012). Report on the 2010 Excavations at Marco Gonzalez, Ambergris Caye. Institute of Archaeology, UCL.

Grigal, D. F. (2003). Mercury sequestration in forests and peatlands. *Journal of Environment Quality*, *32*(2), 393–405. https://doi.org/10.2134/jeq.2003.3930

Guderjan, T. H. (1995). Maya settlement and trade on Ambergris Caye, Belize. *Ancient Mesoamerica*, *6*(1), 147–159. https://doi.org/10.1017/S0956536100002157

Guzmán, H. M., & García, E. M. (2002). Mercury levels in coral reefs along the Caribbean coast of Central America. *Marine Pollution Bulletin*, *44*, 1415–1420. https://doi.org/10.1016/S0025-326X(02)00318-1

Healy, P. F. (1989). Coastal Maya trade. In H. I. McKillop & P. F. Healy (Eds.), *Occasional papers in anthropology*. Issue 8 (pp. 155–164). Trent University.

Hojdová, M., Rohovec, J., Chrastný, V., Penížek, V., & Navrátil, T. (2015). The influence of sample drying procedures on mercury concentrations analyzed in soils. *Bulletin of Environmental Contamination and Toxicology*, *94*(5), 570–576. https://doi.org/10.1007/s00128-015-1521-9

Heiri, O., Lotter, A. F., & Lemcke, G. (2001). Loss on ignition as a method for estimating organic and carbonate content in sediments: Reproducibility and comparability of results. *Journal of Paleolimnology*, *25*(1), 101–110.

King, R. J. (2002). Cinnabar. *Geology Today*, *18*(5), 195–199. https://doi.org/10.1046/j.0266-6979.2003.00366.x

Kongchum, M., Devai, I., DeLaune, R. D., & Jugsujinda, A. (2006). Total mercury and methylmercury in freshwater and salt marsh soils of the Mississippi river deltaic plain. *Chemosphere*, *63*(8), 1300–1303. https://doi.org/10.1016/j.chemosphere.2005.09.024

Krammer, K., & Lange-Bertalot, H. (1988). Bacillariophyceae: Teil 2: Bacillariaceae, Epithemiaceae, Surirellaceae. In Süsswasserflora von Mitteleuropa, Band 2/2.

Krammer, K., & Lange-Bertalot, H. (1991). Bacillariophyceae. 2/3: Centrales, Fragilariaceae, Eunotiaceae. In Süsswasserflora von Mitteleuropa.

Lacerda, L., Soares, T., Costa, B., & Godoy, M. (2011). Mercury emission factors from intensive shrimp aquaculture and their relative importance to the Jaguaribe River Estuary, NE Brazil. *Bulletin of Environmental Contamination and Toxicology*, *87*(6), 657–661. https://doi.org/10.1007/s00128-011-0399-4

Lamoureux-St-Hilaire, M., Canuto, M. A., Wells, E. C., Cagnato, C., & Barrientos, T. (2019). Ancillary economic activities in a Classic Maya regal palace: A multiproxy approach. *Geoarchaeology*, *34*, 768–782. https://doi.org/10.1002/gea.21750

Laperche, V., Hellal, J., Maury-Brachet, R., Joseph, B., Laporte, P., Breeze, D., & Blanchard, F. (2014). Regional distribution of mercury in sediments of the main rivers of French Guiana (Amazonian basin). *SpringerPlus*, *3*, 322. https://doi.org/10.1186/2193-1801-3-322

LeCount, L. J., Christian Wells, E., Jamison, T., & Mixter, D. (2016). Geochemical characterization of inorganic residues on plaster floors from a Maya palace complex at Actuncan, Belize. *Journal of Archaeological Science: Reports*, *5*, 453–464. https://doi.org/10.1016/j.jasrep.2015.12.022

Lentz, D. L., Graham, E., Vinaja, X., Slotten, V., & Jain, R. (2016). Agroforestry and ritual at the ancient Maya center of Lamanai. *Journal of Archaeological Science: Reports*, *8*, 284–294. https://doi.org/10.1016/j.jasrep.2016.06.030

Luzzadder-Beach, S., Beach, T., Terry, R. E., & Doctor, K. Z. (2011). Elemental prospecting and geoarchaeology in Turkey and Mexico. *Catena*, *85*(2), 119–129. https://doi.org/10.1016/j.catena.2010.09.001

Machado, W., Moscatelli, M., Rezende, L. G., & Lacerda, L. D. (2002). Mercury, zinc, and copper accumulation in mangrove sediments surrounding a large landfill in southeast Brazil. *Environmental Pollution*, *120*(2), 455–461. https://doi.org/10.1016/S0269-7491(02)00108-2

Macphail, R. I., Graham, E., Crowther, J., & Turner, S. (2016). Marco Gonzalez, Ambergris Caye, Belize: A geoarchaeological record of ground raising associated with surface soil formation and the presence of a Dark Earth. *Journal of Archaeological Science*, *77*, 35–51. https://doi.org/10.1016/j.jas.2016.06.003

Maher, B., Meng, X., Derbyshire, E., & Kemp, R. A. (1999). Comments on "Origin of the magnetic susceptibility signal in Chinese loess" (multiple letters). *Quaternary Science Reviews*, *18*(6), 865–869. https://doi.org/10.1016/S0277-3791(98)00108-5

Mazzullo, S. J. (2006). Late Pliocene to Holocene platform evolution in northern Belize, and comparison with coeval deposits in southern Belize and the Bahamas. *Sedimentology*, *53*(5), 1015–1047.

McCloskey, T. A., & Keller, G. (2009). 5000 year sedimentary record of hurricane strikes on the central coast of Belize. *Quaternary International*, *195*(1–2), 53–68. https://doi.org/10.1016/j.quaint.2008.03.003

Mckee, K. L., Cahoon, D. R., & Feller, I. C. (2007). Caribbean mangroves adjust to rising sea level through biotic controls on change in soil elevation. *Global Ecology and Biogeography*, *16*(5), 545–556. https://doi.org/10.1111/j.1466-8238.2007.00317.x

McKillop, H. (1984). Prehistoric Maya reliance on marine resources: Analysis of a midden from Moho Cay, Belize. *Journal of Field Archaeology*, *11*(1), 25–35. https://doi.org/10.2307/529338

McKillop, H. (2005). Finds in Belize document Late Classic Maya salt making and canoe transport. *Proceedings of the National Academy of Sciences of the United States of America*, *102*(15), 5630–5634. https://doi.org/10.1073/pnas.0408486102

Mitchell, C. P. J., & Gilmour, C. C. (2008). Methylmercury production in a Chesapeake Bay salt marsh. *Journal of Geophysical Research: Biogeosciences*, *113*, G00C04. https://doi.org/10.1029/2008jg000765

Morin, S., Cordonier, A., Lavoie, I., Arini, A., Blanco, S., Duong, T. T., Tornés, E., Bonet, B., Corcoll, N., Faggiano, L., Laviale, M., Pérès, F., Becares, E., Coste, M., Feurtet-Mazel, A., Fortin, C., Guasch, H., & Sabater, S. (2012). Consistency in diatom response to metal-contaminated environments, H. Guasch A. Ginebreda & A. Geiszinger *Handbook of environmental chemistry* (pp. 117–146). Springer Verlag. https://doi.org/10.1007/978-3-642-25722-3_5

Murray, M. R., Zisman, S. A., & Minty, C. D. (1999). Soil-plant relationships and a revised vegetation classification of Turneffe Atoll, Belize. *Atoll Research Bulletin*, *464*, 1–32. https://doi.org/10.5479/si.00775630.464.1

O'Driscoll, N. J., Canário, J., Crowell, N., & Webster, T. (2011). Mercury speciation and distribution in coastal wetlands and tidal mudflats: Relationships with sulphur speciation and organic carbon. *Water, Air,*

and Soil Pollution, *220*(1–4), 313–326. https://doi.org/10.1007/s11270-011-0756-2

Oonk, S., Slomp, C. P., Huisman, D. J., & Vriend, S. P. (2009). Effects of site lithology on geochemical signatures of human occupation in archaeological house plans in the Netherlands. *Journal of Archaeological Science*, *36*(6), 1215–1228. https://doi.org/10.1016/j.jas.2009.01.010

O'Shea, F. T., Cundy, A. B., & Spencer, K. L. (2018). The contaminant legacy from historic coastal landfills and their potential as sources of diffuse pollution. *Marine Pollution Bulletin*, *128*, 446–455. https://doi.org/10.1016/j.marpolbul.2017.12.047

Pande, A., Nayak, G. N., Prasad, V., & PrakashBabu, C. (2015). Geochemical and diatom records of recent changes in depositional environment of a tropical wetland, central west coast of India. *Environmental Earth Sciences*, *73*(9), 5447–5461. https://doi.org/10.1007/s12665-014-3799-z

Parnell, J. J., Terry, R. E., & Nelson, Z. (2002). Soil chemical analysis applied as an interpretive tool for ancient human activities in Piedras Negras, Guatemala. *Journal of Archaeological Science*, *29*(4), 379–404. https://doi.org/10.1006/jasc.2002.0735

Parsons, M. L., Dortch, Q., Turner, R. E., & Rabalais, N. R. (2006). Reconstructing the development of eutrophication in Louisiana salt marshes. *Limnology and Oceanography*, *51*, 534–544. https://doi.org/10.4319/lo.2006.51.1_part_2.0534

Pendergast, D. M. (1982). Ancient Maya mercury. *Science*, *217*(4559), 533–535.

Reimann, C., Filzmoser, P., & Garrett, R. G. (2005). Background and threshold: Critical comparison of methods of determination. *Science of the Total Environment*, *346*(1), 1–16.

Reimann, C., & de Caritat, P. (2005). Distinguishing between natural and anthropogenic sources for elements in the environment: Regional geochemical surveys versus enrichment factors. *Science of the Total Environment*, *337*(1-3), 91–107. https://doi.org/10.1016/j.scitotenv.2004.06.011

Roobol, M. J., & Smith, A. L. (1980). Pumice eruptions of the lesser Antilles. *Bulletin Volcanologique*, *43*(2), 277–286. https://doi.org/10.1007/BF02598032

Rood, B. E., Gottgens, J. F., Delfino, J. J., Earle, C. D., & Crisman, T. L. (1995). Mercury accumulation trends in Florida Everglades and Savannas Marsh flooded soils. *Water, Air, & Soil Pollution*, *80*(1–4), 981–990. https://doi.org/10.1007/BF01189752

Rosales-Hoz, L., Cundy, A. B., & Bahena-Manjarrez, J. L. (2003). Heavy metals in sediment cores from a tropical estuary affected by anthropogenic discharges: Coatzacoalcos estuary, Mexico. *Estuarine, Coastal and Shelf Science*, *58*(1), 117–126. https://doi.org/10.1016/S0272-7714(03)00066-0

Rose, N. L. (2008). Quality control in the analysis of lake sediments for spheroidal carbonaceous particles. *Limnology and Oceanography-Methods*, *6*, 172–179. https://doi.org/10.4319/lom.2008.6.172

Rose, N. L., & Juggins, S. (1994). A spatial relationship between carbonaceous particles in lake sediments and sulphur deposition. *Atmospheric Environment*, *28*(2), 177–183. https://doi.org/10.1016/1352-2310(94)90092-2

Rudnick, R. L., & Gao, S. (2003). Composition of the continental crust, H. Holland & K. Turekian *Treatise on Geochemistry* (Vol. 3–9, pp. 1–64). Elsevier Inc. https://doi.org/10.1016/B0-08-043751-6/03016-4

Rúa, A., Liebezeit, G., & Palacio-Baena, J. (2014). Mercury colonial footprint in Darién Gulf sediments, Colombia. *Environmental Earth Sciences*, *71*, 1781–1789. https://doi.org/10.1007/s12665-013-2583-9

Sills, E. C., & McKillop, H. (2018). Specialized salt production during the ancient Maya Classic Period at two Paynes Creek Salt Works, Belize: Chan b'i and Atz'aam Na. *Journal of Field Archaeology*, *43*(6), 457–471. https://doi.org/10.1080/00934690.2018.1504543

Sills, E. C., McKillop, H., & Wells, E. C. (2016). Chemical signatures of ancient activities at Chan b'i—A submerged Maya salt works, Belize. *Journal of Archaeological Science: Reports*, *9*, 654–662. https://doi.org/10.1016/j.jasrep.2016.08.024

Silva, L. F. F., Machado, W., Lisboa Filho, S. D., & Lacerda, L. D. (2003). Mercury accumulation in sediments of a mangrove ecosystem in SE Brazil. *Water, Air, and Soil Pollution*, *145*(1–4), 67–77. https://doi.org/10.1023/A:1023610623280

Simmons, S. E., & Graham, E. (2017). Maya coastal adaptations in Classic and Postclassic times on Ambergris Caye, Belize. In M. Patton, & J. Manion (Eds), *Trading Spaces: The Archaeology of Interaction, Migration and Exchange. Proceedings of the 46th Annual Chacmool Archaeology Conference* (pp. 167-180). Chacmool Archaeology Association, University of Calgary.

Simmons, S. E., Mayfield, T., Aimers, J. J., & Stemp, W. J. (2018). The Maya of Ambergris Caye and their neighbors. *Research Reports in Belizean Archaeology*, *15*, 329–339.

Stidolph, S., Sterrenburg, F., Smith, K., & Kraberg, A. (2012). Stuart R. Stidolph Diatom Atlas. *U.S. Geological Survey Open-File Report*, 2012–1163. https://pubs.usgs.gov/of/2012/1163/index.html

Teixeira, D. C., Montezuma, R. C., Oliveira, R. R., & Silva-Filho, E. V. (2012). Litterfall mercury deposition in Atlantic forest ecosystem from SE-Brazil. *Environmental Pollution*, *164*, 11–15. https://doi.org/10.1016/j.envpol.2011.10.032

Terry, R. E., Fernandez, F. G., Parnell, J. J., & Inomata, T. (2004). The story in the floors: Chemical signatures of ancient and modern Maya activities at Aguateca, Guatemala. *Journal of Archaeological Science*, *31*(9), 1237–1250. https://doi.org/10.1016/j.jas.2004.03.017

Vos, P. C., & de Wolf, H. (1993). Reconstruction of sedimentary environments in Holocene coastal deposits of the southwest Netherlands; the Poortvliet boring, a case study of palaeoenvironmental diatom research. *Hydrobiologia*, *269–270*, 297–306. https://doi.org/10.1007/BF00028028

Wang, C., Pan, D., Han, H., & Hu, X. (2018). Vertical profile, contamination assessment of mercury and arsenic in sediment cores from typical intertidal zones of China. *Environmental Monitoring and Assessment*, *190*(6), 366. https://doi.org/10.1007/s10661-018-6732-1

Wells, E. C., Terry, R. E., Parnell, J. J., Hardin, P. J., Jackson, M. W., & Houston, S. D. (2000). Chemical analyses of ancient anthrosols in residential areas at Piedras Negras, Guatemala. *Journal of Archaeological Science*, *27*(5), 449–462. https://doi.org/10.1006/jasc.1999.0490

Williams, J. S., White, C. D., & Longstaffe, F. J. (2009). Maya marine subsistence: Isotopic evidence from Marco Gonzalez and San Pedro, Belize. *Latin American Antiquity*, *20*(1), 37–56. https://doi.org/10.1017/S1045663500002509

Wilson, C. A., Davidson, D. A., & Cresser, M. S. (2008). Multi-element soil analysis: An assessment of its potential as an aid to archaeological interpretation. *Journal of Archaeological Science*, *35*(2), 412–424. https://doi.org/10.1016/j.jas.2007.04.006

SUPPORTING INFORMATION

Additional Supporting Information may be found online in the supporting information tab for this article.

How to cite this article: Turner, S., Graham, E., MacPhail, R., Duncan, L., Rose, N. L., Yang, H., Whittet, R., & Rosique-Esplugas, C. (2021). Mercury enrichment in anthrosols and adjacent coastal sediments at a Classic Maya site, Marco Gonzalez, Belize *Geoarchaeology*, 1–22. https://doi.org/10.1002/gea.21868